PHYSICAL REVIEW B VOLUME 18, NUMBER 12 15 DECEMBER 1978

Phonon focusing and phonon conduction in orthorhombic and tetragonal crystals in the boundary-scattering regime. II

C. G. Winternheimer*† and A. K. McCurdy
Electrical Engineering Department, Worcester Polytechnic Institute, Worcester, Massachusetts 01609
(Received 12 September 1977)

Striking differences (up to a factor of 100) are predicted in the intensity of phonons propagating ballistically along different directions in certain orthorhombic and tetragonal crystals. The predicted results arise from phonon focusing due to elastic anisotropy, due to the fact that in elastically anisotropic crystals the phonon phase and group velocities are, in general, not collinear. Conditions for the existence of cuspidal edges in group-velocity surfaces are given in symmetry planes along all directions where the phase and group velocities are collinear. Approximate amplification factors have been calculated for phonons of each polarization along symmetry-plane collinear axes. An analytic expression is also given for the nonsymmetry collinear direction for the longitudinal and one of the transverse modes. Calculations have been performed for a number of crystals and demonstrate that the phonon-focusing property can cause differences in the phonon transport in the boundary-scattering regime by more than 80%.

I. INTRODUCTION

Thermal energy in dielectric solids is carried by phonons. At sufficiently low temperatures the phonons propagate ballistically so that in the absence of defect or impurity scattering the mean free path becomes limited by the linear dimensions of the sample.[1] A theory of the thermal conductivity applicable to this temperature range was first developed by Casimir.[2] Corrections to Casimir's theory have been derived for samples of finite length,[3] for samples in which a fraction of the phonon are specularly reflected from the end surfaces,[4] and for samples in which phonon focusing is important.[5,6]

For superconducting metals in the temperature range $T/T_c \ll 1$, there are negligible normal-state electrons to carry heat[7] so that thermal transport is dominated by phonon-scattering processes. At the lowest temperatures where the electronic scattering of phonons can be insignificant, the phonon mean free path becomes limited by scattering from sample boundaries and crystal imperfections. For a sufficiently defect-free superconductor, i.e., $\Lambda_{ph} \sim l$, the thermal conductivity at $T/T_c \ll 1$ should be determined by the same factors as in a dielectric crystal. This is indicated in the most recent measurements on niolium[8] where at lowest temperatures $\Lambda_{ph} \sim l$, and the thermal conductivity was proportional to T^3, characteristic of the Casimir result.

Recent heat-pulse measurements[9,10] have shown striking differences in the intensity of phonons propagating ballistically in an elastically anisotropic crystal. These results were shown to arise from phonon focusing due to the fact that the phase and group velocities are not collinear except along certain axes. It is only along these axes that the energy flow or ray vector is in the same direction as the wave vector. Because of elastic anisotropy the angular deviation between the phase and group velocities varies with the direction of the wave vector. Phonon focusing occurs when the direction of the group velocity varies more slowly than in an elastically isotropic solid. Furthermore, for certain ratios between the elastic constants, two or more wave vectors can give rise to the same group-velocity direction and the group-velocity surface is said to have cuspidal edges. Conditions for cuspidal edges have been derived by Musgrave,[11] Maris,[12] and McCurdy.[13] Maris[12] has pointed out that the presence of cusps increases the phonon intensity, particularly along the edges where the direction of the group velocity varies slowly with wave vector. As a result the energy flow is enhanced about cuspidal or highly focused directions and significantly decreased along other directions.

Subsequent measurements of the thermal conductivity of silicon and calcium fluoride in the boundary-scattering regime demonstrated anisotropies of up to 50% for silicon and 40% for calcium fluoride.[5,6] The predictions of Casimir's theory, generalized to allow for phonon focusing, gave quantitative agreement with experimental results. Similar anisotropies in the thermal conductivity have been predicted for sufficiently defect-free, superconducting lead and niobium at $T/T_c \ll 1$.[14]

Phonon-focusing effects have also been predicted in elastically anisotropic hexagonal crystals.[13] Subsequent heat-pulse measurements in solid ^{4}He by Narayanamurti and Dynes[15] indicated a phonon intensity approximately 45° to the c axis, consistent with predictions of a cuspidal edge.[13] Calcu-

lations of thermal conductivity also show that effects of focusing can actually reverse the anisotropy one obtains by neglecting the angular deviation between the phase and group velocities.[13,14]

In this paper phonon-focusing effects are studied in orthorhombic and tetragonal crystals. Results derived for the hexagonal lattice[13] (hereafter referred as paper I) are generalized to include all the symmetry planes of the orthorhombic, tetragonal, and cubic lattices. Conditions for phonon focusing, and for the existence of cuspidal edges about collinear axes, are given for wave vectors in symmetry planes. Approximate phonon amplification factors are calculated for phonons of each polarization along high-symmetry collinear axes. Calculations of phonon focusing are given for a number of crystals, and calculations of thermal conductivity are given for one orthorhombic, one tetragonal, and one cubic crystal. Strong phonon focusing is predicted to have a dramatic effect upon the phonon conductivity. For sufficiently defect-free solids, this should be observable in dielectrics at temperatures which are a small fraction of the Debye temperature, but for superconductors at temperatures which are a small fraction of the superconducting transition temperature.

II. THEORY

A. Calculation of phonon phase and group velocities

The solutions for the phonon phase velocities in the symmetry planes of the orthorhombic, tetragonal, cubic, and hexagonal elastic solids are well known.[16-18] For any symmetry plane of these lattices the phonon phase velocities can be expressed in terms of generalized elastic constants as[19]

$$s_1^2=(a_1\sin^2\theta_k+a_2\cos^2\theta_k)/\rho \tag{1}$$

and

$$s_{0,2}^2=\tfrac{1}{2}\rho\{(a_3\sin^2\theta_k+a_4\cos^2\theta_k) \pm|[(a_5\sin^2\theta_k-a_6\cos^2\theta_k)^2+(2a_7\sin\theta_k\cos\theta_k)^2]^{1/2}|\}. \tag{2}$$

The displacement vector $\vec{u}$, giving the direction of the deformation for wave vectors in symmetry planes, is given by[20]

$$\vec{u}_1=(\vec{e}\times\vec{n})/[1-(\vec{e}\cdot\vec{n})^2]^{1/2}, \tag{3}$$

$$\vec{u}_{0,2}=\vec{n}-\left(\frac{a_5\sin^2\theta_k+(2a_7-a_6)\cos^2\theta_k}{2a_7\cos\theta_k}\mp\frac{|[(a_5\sin^2\theta_k-a_6\cos^2\theta_k)^2+(2a_7\sin\theta_k\cos\theta_k)^2]^{1/2}|}{2a_7\cos\theta_k}\right)\vec{e}. \tag{4}$$

In these equations, s is the phase velocity, ρ is the density, the a_i are second-order elastic constants or linear combinations of these constants, $\vec{n}$ is a unit vector in the direction of the wave vector, and $\vec{e}$ is a unit vector parallel to the $\vec{\eta}$ axis. The angle θ_k gives the angular direction of the wave vector in a symmetry plane measured with respect to the η axis. For any symmetry plane containing the z axis, the η axis is chosen parallel to the [001] direction, but for the (001) symmetry plane the η axis is chosen parallel to the [100] direction. Expressions for the generalized constants a_i for each of the symmetry planes of the orthorhombic, tetragonal, and cubic lattices are given in Table I.[21] Expressions for the hexagonal lattice for symmetry planes containing the c axis are also included in this table. The subscripts 0, 1, 2 on the phase velocity and the displacement vector refer to the different modes of propagation which will be designated as the fast, transverse T_1, and slow modes, respectively.[22] The sign preceding the radical in Eq. (2) is positive for the fast mode and negative for the slow mode, but is negative for the fast mode and positive for the slow mode in Eq. (4). Note that $2\rho s^2=a_4+|a_6|$ for the fast mode, but $a_4-|a_6|$ for the slow mode when $\theta_k=0°$, and that $2\rho s^2=a_3+|a_5|$ for the fast mode, but $a_3-|a_5|$ for the slow mode when $\theta_k=90°$ so that the fast mode is always of higher velocity than the slow mode. A schematic diagram of ρs^2 for each of the different modes in an orthorhombic lattice is shown in Fig. 1. The ρs^2 surfaces for a tetragonal crystal are shown in Fig. 2.

Conditions for elastic stability place restrictions on the constants a_i. In order for a solid to be elastically stable the determinant $|C_{\alpha\beta}|$ of the elastic matrix must be positive. This in turn requires that the sequential principal minors be positive.[23] Furthermore, since an identical permutation of the rows and columns of the determinant $|C_{\alpha\beta}|$ can bring any principal minor to the top left corner, there are three equivalent sets of conditions for elastic stability in the orthorhombic lattice. These are given by inequalities (6). For the orthohombic lattice

$$C_{11}>0,\quad C_{22}>0,\quad C_{33}>0,\quad C_{44}>0,\quad C_{55}>0,\quad C_{66}>0, \tag{5}$$

$$C_{11}C_{22}>C_{12}^2 \text{ or } C_{11}C_{33}>C_{13}^2 \text{ or } C_{22}C_{33}>C_{23}^2, \tag{6}$$

and

$$C_{33}(C_{11}C_{12}-C_{12}^2)^2 > C_{23}^2C_{11}+C_{13}^2C_{22}-2C_{12}C_{13}C_{23}. \tag{7}$$

In the tetragonal lattice there are only two equivalent sets of conditions for stability. These are inequalities (9). For the tetragonal lattice

$$C_{33}>0, \quad C_{44}>0, \quad C_{66}>0, \tag{8}$$

$$C_{11}>|C_{12}| \text{ or } C_{11}C_{33}>C_{13}^2, \tag{9}$$

and

$$C_{33}(C_{11}+C_{12})>2C_{13}^2. \tag{10}$$

Since $C_{11}>|C_{12}|$ it follows that $C_{11}>(C_{11}+C_{12})/2>0$ so that inequalities (9) and (10) can be written as

$$C_{11}C_{33}>C_{33}(C_{11}+C_{12})/2>C_{13}^2. \tag{11}$$

In a similar way, conditions for elastic stability in the hexagonal lattice can be expressed as

$$C_{33}>0, \quad C_{44}>0 \tag{12}$$

nd

$$C_{11}C_{33}>C_{33}(C_{11}+C_{12})/2>C_{13}^2, \tag{13}$$

and for the cubic lattice as

$$C_{11}>0, \quad C_{44}>0 \tag{14}$$

and

$$C_{11}^2>C_{11}(C_{11}+C_{12})/2>C_{12}^2. \tag{15}$$

In hexagonal crystals $C_{66}=(C_{11}-C_{12})/2$ so that inequality (13) can be written as

$$C_{11}C_{33}>C_{33}(C_{11}-C_{66})>C_{13}^2, \tag{16}$$

which requires $C_{11}>C_{66}$, whereas $C_{11}<C_{66}$ in one known tetragonal crystal, paratellurite.

The above conditions require $a_1>0$, $a_2>0$, $a_3>0$, and $a_4>0$. Since it is physically more reasonable, a_7 will be chosen positive.[24] Constants a_5 and a_6 are greater than zero for all known materials with one recently discovered exception, paratellurite, a tetragonal piezoelectric crystal.[25,26] In this material at room temperature $C_{66}>C_{11}$, so that a_5 and a_6 are negative in the (001) symmetry plane. As a result the fast mode is quasitransverse and the slow mode quasilongitudinal in the (001) plane near the [100] and [010] directions. Furthermore, since $C_{66}>C_{11}$, $a_1>(a_3+a_5)/2$ for the (010) or (100) symmetry planes so that the

TABLE I. Values of the generalized elastic constants in symmetry planes of orthorhombic, tetragonal, hexagonal, and cubic crystals.

	Orthorhombic Symmetry Planes		
	(010)	(100)	(001)
a_1	C_{66}	C_{66}	C_{44}
a_2	C_{44}	C_{55}	C_{55}
a_3	$C_{11}+C_{55}$	$C_{22}+C_{44}$	$C_{22}+C_{66}$
a_4	$C_{33}+C_{55}$	$C_{33}+C_{44}$	$C_{11}+C_{66}$
a_5	$C_{11}-C_{55}$	$C_{22}-C_{44}$	$C_{22}-C_{66}$
a_6	$C_{33}-C_{55}$	$C_{33}-C_{44}$	$C_{11}-C_{66}$
a_7	$C_{13}+C_{55}$	$C_{23}+C_{44}$	$C_{12}+C_{66}$
	Tetragonal Symmetry Planes		
	(010) or (100)	(110)	(001)
a_1	C_{66}	$\frac{1}{2}(C_{11}-C_{12})$	C_{44}
a_2	C_{44}	C_{44}	C_{44}
a_3	$C_{11}+C_{44}$	$\frac{1}{2}(C_{11}+C_{12})+C_{66}+C_{44}$	$C_{11}+C_{66}$
a_4	$C_{33}+C_{44}$	$C_{33}+C_{44}$	$C_{11}+C_{66}$
a_5	$C_{11}-C_{44}$	$\frac{1}{2}(C_{11}+C_{12})+C_{66}-C_{44}$	$C_{11}-C_{66}$
a_6	$C_{33}-C_{44}$	$C_{33}-C_{44}$	$C_{11}-C_{66}$
a_7	$C_{13}+C_{44}$	$C_{13}+C_{44}$	$C_{12}+C_{66}$
	Hexagonal Plane containing [001] axis	Cubic Symmetry Planes {100}	{110}
a_1	C_{66}	C_{44}	$\frac{1}{2}(C_{11}-C_{12})$
a_2	C_{44}	C_{44}	C_{44}
a_3	$C_{11}+C_{44}$	$C_{11}+C_{44}$	$\frac{1}{2}(C_{11}+C_{12})+2C_{44}$
a_4	$C_{33}+C_{44}$	$C_{11}+C_{44}$	$C_{11}+C_{44}$
a_5	$C_{11}-C_{44}$	$C_{11}-C_{44}$	$\frac{1}{2}(C_{11}+C_{12})$
a_6	$C_{33}-C_{44}$	$C_{11}-C_{44}$	$C_{11}-C_{44}$
a_7	$C_{13}+C_{44}$	$C_{12}+C_{44}$	$C_{12}+C_{44}$

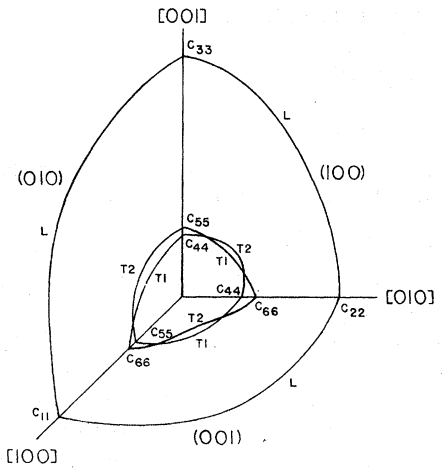

FIG. 1. ρs^2 surfaces of orthorhombic gallium in symmetry planes. In this material a_5 and $a_6 > 0$ for all three symmetry planes. Note particularly the interesting character of the phase velocity surface, for example, where ρs^2 equals C_{55} in the [001] direction. This surface is T_1 in the (100) plane but T_2 in the (010) plane.

phase velocity of the transverse T_1 mode exceeds the phase velocity of the fast mode along the [100] and [010] axes.

From Eq. (4) it can be seen that if $a_5 > 0$ the fast mode is quasilongitudinal and the slow mode quasitransverse[27] near $\eta_\perp$, but if $a_5 < 0$ the fast mode is quasitransverse and the slow mode quasilongitudinal near this direction. Similarly, if $a_6 > 0$ the fast mode is quasilongitudinal and the slow mode

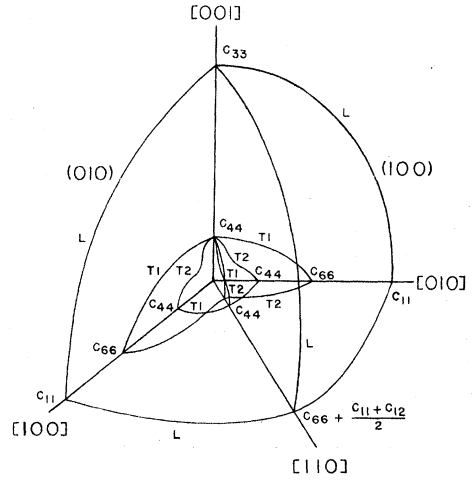

FIG. 2. ρs^2 surfaces of tetragonal indium in symmetry planes. In this material a_5 and $a_6 > 0$ for all three symmetry planes. Note in this case, because of the equivalence of the [100] and [010] axes, the phase-velocity modes in the (100) and (010) planes are the same in the [001] direction. The abscissa of the T_2 surface in the (001) plane along the [110] axis is $\frac{1}{2}(C_{11}-C_{12})$.

quasitransverse near the η axis, but if $a_6 < 0$ the fast mode is quasitransverse and the slow mode quasilongitudinal near this axis.

In symmetry planes the components of group velocity parallel and perpendicular to the η axis, respectively, can be determined using the relations[28]

$$v_\parallel = \frac{\partial s}{\partial(\cos\theta_k)} \quad \text{and} \quad v_\perp = \frac{\partial s}{\partial(\sin\theta_k)}. \tag{17}$$

The direction θ_v of the group velocity can then be determined by the relation

$$\tan\theta_v = v_\perp / v_\parallel . \tag{18}$$

For the T_1 mode this expression becomes

$$\tan\theta_v = (a_1/a_2)\tan\theta_k$$

or

$$\cot\theta_v = (a_2/a_1)\cot\theta_k , \tag{19}$$

and for the fast and slow modes

$$\tan\theta_v = (u/v)\tan\theta_k , \tag{20}$$

where

$$u = a_3 \pm \frac{a_5^2\tan^2\theta_k + 2a_7^2 - a_5a_6}{|[(a_5\tan^2\theta_k - a_6)^2 + (2a_7\tan\theta_k)^2]^{1/2}|} , \tag{21}$$

$$v = a_4 \pm \frac{(2a_7^2 - a_5a_6)\tan^2\theta_k + a_6^2}{|[(a_5\tan^2\theta_k - a_6)^2 + (2a_7\tan\theta_k)^2]^{1/2}|} , \tag{22}$$

with the "+" sign used for fast waves and the "−" sign for slow waves.

For directions nearly perpendicular to the η axis it is more convenient to use

$$\cot\theta_v = (u'/v')\cot\theta_k , \tag{23}$$

where u' is u and v' is v, but with a_3 and a_4 interchanged, a_5 and a_6 interchanged, and with $\cot\theta_k$ replacing $\tan\theta_k$.

The angular deviation between the group and phase velocities can be written in the convenient form[29,30]

$$\tan(\theta_v - \theta_k) = \frac{1}{s}\frac{\partial s}{\partial\theta_k} = \frac{1}{2s^2}\frac{\partial s^2}{\partial\theta_k} . \tag{24}$$

These equations make it possible to calculate the angle between the phase and group velocities for each mode along all wave-vector directions in symmetry planes. In elastically anisotropic crystals the phonon phase and group velocities are collinear for only certain directions determined by the symmetry and the kind of anisotropy.

For certain ratios between the elastic constants it is possible to find values of θ_v for the slow mode which permit more than one corresponding value of θ_k. In these regions the values of θ_k can be double or triple valued and the group-velocity sur-

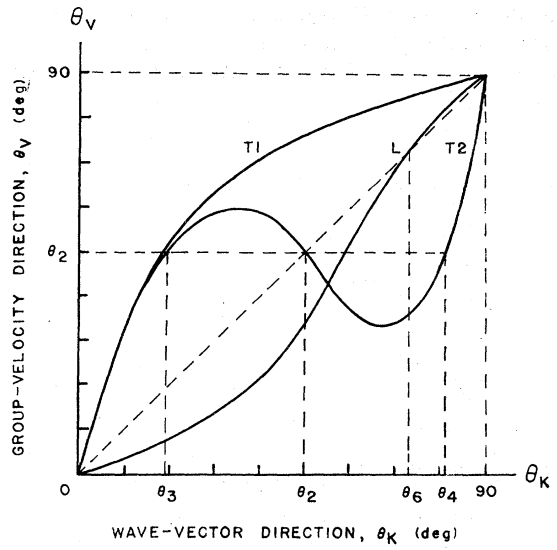

FIG. 3. Relation between the direction of the wave vector and the group-velocity vector in the (001) plane for orthohombic potassium pentaborate using the elastic constants of Cook and Jaffe. Angles are measured with respect to the [100] axis. Note the negative slope of the T_2 curve near θ_2, indicating a cusp about that direction. Wave vectors in directions θ_2, θ_3, and θ_4 all give rise to group-velocity vectors in the θ_2 direction.

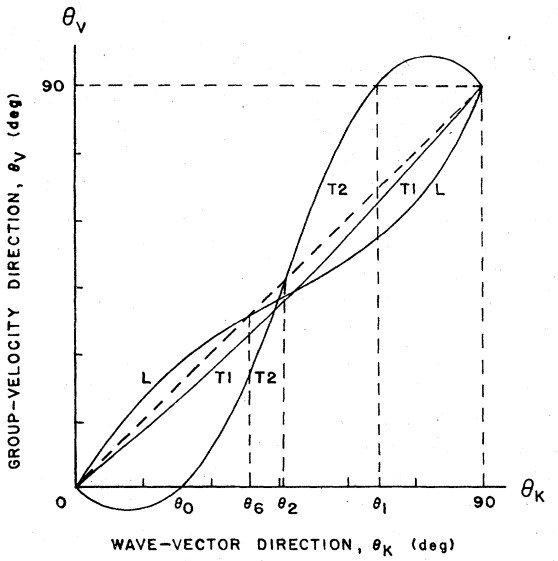

FIG. 4. Relation between the direction of the wave vector and the group-velocity vector in the (001) plane of gallium using the elastic constants of Lyall and Cochran. Angles are measured with respect to the [100] axis. Note the cuspidal edges in the T_2 mode about the [100] and [010] axes.

face is said to have cuspidal edges (see Figs. 3 and 4).

Cuspidal edges can occur not only when the wave vectors are confined to symmetry planes, but also for wave vectors on either side of a symmetry plane. In the orthorhombic lattice there are collinear directions, not contained in any symmetry plane, about which cuspidal edges can occur. Cuspidal edges occurring for wave vectors confined to symmetry planes are discussed in Sec. II D. Cuspidal edges occurring for wave vectors on either side of a symmetry plane are discussed in Sec. III.

B. Calculations of collinear and pure-mode axes

A collinear axis will be defined as one along which the phase velocity or wave vector and the corresponding group velocity or ray vector are collinear. It should be emphasized that *only* along these axes is the flow of energy in the same direction as the wave vector. Since collinearity requires $\theta_v = \theta_k$, Eq. (24) shows that collinear points in symmetry planes are points where $\partial s/\partial\theta_k$ is zero and thus, are points of tangency to the phase-velocity surface. A pure-mode axis, however, is one along which the displacement or polarization vector and the wave vector are parallel for a pure longitudinal wave or perpendicular for pure transverse waves. Since the three polarization vectors are mutually perpendicular for each value of the wave vector, a pure-mode axis is a direction along which a pure longitudinal and two pure transverse waves propagate. Pure-mode axes for a number of crystal symmetries have been given by Brugger.[31] Although pure modes propagate in general only for wave vectors parallel to the x, y, and z axes, directions which incidently are also collinear axes for all modes, pure transverse and pure longitudinal waves also propagate along all longitudinal (collinear) axes.

The solution for the collinear axes in symmetry planes can be obtained from Eqs. (20)–(22). It is clear that the transverse T_1 mode, although a pure transverse wave, has no collinear axes except for $\theta_k = 0^0$ and 90^0 unless $a_1 = a_2$, in which case this mode is collinear for all wave-vector directions in that symmetry plane. The solution for the collinear axes for the fast and slow modes in symmetry planes yields the values $\theta_k = 0^0$ and 90^0 required by symmetry, as well as a quadratic equation in $\tan^2\theta_k$, whose roots are

$$\tan^2\theta_k = (a_6 + a_7)/(a_5 + a_7)$$

or

$$\tan^2\theta_k = (a_6 - a_7)/(a_5 - a_7).$$

The collinear axis θ_s for the slow mode which in

general is quasitransverse[32] near θ_s is

$$\tan\theta_s=[(a_6+|a_7|)/(a_5+|a_7|)]^{1/2}, \tag{25}$$

and the collinear axis θ_f for the fast mode which is pure longitudinal at θ_f is

$$\tan\theta_f=[(a_6-|a_7|)/(a_5-|a_7|)]^{1/2}. \tag{26}$$

Equation (26) thus gives the collinear axis for the longitudinal mode and the direction along which a pure longitudinal and two pure transverse waves propagate.

For nonsymmetry planes solutions for the collinear axes can be found using the defining relations

$$\begin{aligned} s_x&=ls=v_x=\frac{\partial s}{\partial l},\\ s_y&=ms=v_y=\frac{\partial s}{\partial m},\\ s_z&=ns=v_z=\frac{\partial s}{\partial n}; \end{aligned} \tag{27}$$

thus the direction cosines of the collinear axes can be expressed as

$$l=\frac{1}{s}\frac{\partial s}{\partial l},\quad m=\frac{1}{s}\frac{\partial s}{\partial m},\quad n=\frac{1}{s}\frac{\partial s}{\partial n}. \tag{28}$$

Brugger[31] used a method due to Borgnis[33] to derive the relations for the collinear axes for the longitudinal mode. Using the notation in this paper, his results can be expressed as

$$\frac{m}{l}=\left(\frac{a^-_{xz}b^-_{xz}-a^-_{xz}b^-_{yz}-b^-_{xy}b^-_{xz}}{a^-_{yz}b^-_{yz}-a^-_{yz}b^-_{xz}-a^-_{xy}b^-_{yz}}\right)^{1/2}, \tag{29}$$

$$\frac{n}{l}=\left(\frac{a^-_{xy}b^-_{xy}-a^-_{yz}b^-_{xy}-a^-_{xz}a^-_{xy}}{a^-_{yz}b^-_{yz}-a^-_{yz}b^-_{xz}-a^-_{xy}b^-_{yz}}\right)^{1/2}, \tag{30}$$

where

$$\begin{aligned} a^-_{xy}&=(a_5-a_7)_{xy}=C_{22}-2C_{66}-C_{12},\\ a^-_{xz}&=(a_5-a_7)_{xz}=C_{11}-2C_{55}-C_{13},\\ a^-_{yz}&=(a_5-a_7)_{yz}=C_{22}-2C_{44}-C_{23},\\ b^-_{xy}&=(a_6-a_7)_{xy}=C_{11}-2C_{66}-C_{12},\\ b^-_{xz}&=(a_6-a_7)_{xz}=C_{33}-2C_{55}-C_{13},\\ b^-_{yz}&=(a_6-a_7)_{yz}=C_{33}-2C_{44}-C_{23}. \end{aligned} \tag{31}$$

The double-letter subscripts designate the planes in Table I where the values of a_5, a_6, and a_7 are given in terms of the second-order elastic constants. The angle ϕ_f of the collinear axis for the fast mode can be calculated from

$$\tan\phi_f=m/l \tag{32}$$

and the angle θ_f can be found by using

$$\tan\theta_f=l/n\cos\phi_f. \tag{33}$$

For one of the transverse modes, however, the results for the collinear axis are equivalent to a change in the signs of some of the terms in Brugger's expression for the longitudinal mode. These results are

$$\frac{m}{l}=\left(\frac{a^+_{xz}b^+_{xz}-a^+_{xz}b^+_{yz}-b^-_{xy}b^+_{xz}}{a^+_{yz}b^+_{yz}-a^+_{yz}b^+_{xz}-a^-_{xy}b^+_{yz}}\right)^{1/2} \tag{34}$$

and

$$\frac{n}{l}=\left(\frac{a^-_{xy}b^-_{xy}-a^+_{yz}b^-_{xy}-a^+_{xz}a^-_{xy}}{a^+_{yz}b^+_{yz}-a^+_{yz}b^+_{xz}-a^-_{xy}b^+_{yz}}\right)^{1/2}, \tag{35}$$

where

$$\begin{aligned} a^+_{xz}&=(a_5+a_7)_{xz}=C_{11}+C_{13},\\ a^+_{yz}&=(a_5+a_7)_{yz}=C_{22}+C_{23},\\ b^+_{xz}&=(a_6+a_7)_{xz}=C_{33}+C_{13},\\ b^+_{yz}&=(a_6+a_7)_{yz}=C_{33}+C_{23}. \end{aligned} \tag{36}$$

The angles ϕ_s and θ_s of the collinear axis for this transverse mode can be calculated from Eqs. (32) and (33) but with ϕ_s replacing ϕ_f, and θ_s replacing θ_f. Collinear axes for a number of orthorhombic materials are tabulated in Table II. The elastic constants of these materials listed in Table II are tabulated in Table XVI.

C. Approximate phonon-amplification factor for cusp-free velocity surfaces about collinear axes in symmetry planes

A cusp-free surface is one for which there is one and only one wave vector for each group-velocity direction.[34] Since an elastically anisotropic orthorhombic lattice has no transverse isotropy, exact analytic expressions cannot be obtained for the phonon-amplification factor as in the case of the hexagonal lattice. To find the cusp-free phonon-amplification factor for a nonhexagonal lattice consider first a collinear direction which is the intersection of two mutually orthogonal symmetry planes,[35] and consider all the group-velocity directions in a solid angle $\Delta\Omega_v$ subtended by a detector, all points of which are within a small angle $\Delta\theta_v$ from the collinear axis. Each phonon trajectory or group-velocity direction corresponds to a wave vector in a direction $\Delta\theta_k$ from the collinear axis which because of elastic anisotropy is different from $\Delta\theta_v$ both in angular distance from the collinear axis and in azimuthal angle from a reference symmetry plane. The phonon-amplification factor A is defined as the ratio of the solid angle $\Delta\Omega_k$ in wave-vector or k space to the corresponding solid angle $\Delta\Omega_v$ in group-velocity space. If there are no cuspidal edges in the group-velocity surface, then each group-velocity has only one corresponding value of wave vector, and the phonon-amplification factor (PAF) in the collinear

TABLE II. Collinear and pure-mode axes in nonsymmetry planes of orthorhombic crystals. The collinear axis for the longitudinal mode is also a pure-mode axis. Double-starred values were found by a numerical search method; other values were found analytically.

Material	Longitudinal		Collinear axes: Slower T		Faster T	
	θ	ϕ	θ	ϕ	θ	ϕ
Aragonite ($CaCO_3$)[a]	48.55	85.18	...	...	...	...
$BaSO_4$[b]	57.80	28.47	...	...	46.06	47.14
Benzophenone[c]	...	...	...	...	...	...
Gallium (at 4.2 °K)[d]	62.57	35.83	16.73**	31.81**	47.25	43.42
Iodic acid (HIO_3)[e]	39.72	33.21	...	...	...	...
Iodic acid (DIO_3)[e]	39.24	32.21	...	...	...	...
Lithium ammonium tartrate[f]	...	...	...	...	41.42	32.74
$MgSO_4 \cdot 7H_2O$[g]	...	...	44.47	33.54	...	...
$NiSO_4 \cdot 7H_2O$[g]	...	...	44.16	35.42	...	...
Olivine[h]	...	...	...	...	...	...
Potassium pentaborate[i]	61.52	51.17	...	...	58.82**	38.61**
Resorcinol[j]	50.14	47.61	...	...	...	...
Rochelle salt[k]	...	...	...	...	...	...
Sodium ammonium tartrate[l]	...	...	...	...	...	...
Sodium tartrate[k]	...	...	...	...	48.22	18.76
Staurolite[m]	...	...	...	...	62.08**	45.01**
Strontium sulphate[b]	58.31	33.84	36.98**	31.35**	45.83	44.47
Sulfur[n]	67.59	17.60	...	...	58.48**	27.09**
Terpine monohydrate[o]	...	...	61.83**	39.14**	...	...
Topaz[p]	...	...	48.47**	67.16**	42.74	56.84
Uranium (at 4.2 °K)[q]	...	...	...	...	50.18	41.13
$ZnSO_4 \cdot 7H_2O$[g]	...	...	44.66	23.41	...	...

[a] W. Voigt, Ann. Phys. (Leipz.) 24, 290 (1907).
[b] T. Seshagiri Rao, Proc. Indian Acad. Sci. A 33, 251 (1951).
[c] A. A. Chumakov, I. M. Silvestrova, and K. S. Aleksandrov, Kristallografiya 2, 707 (1957) [Sov. Phys.-Crystallogr. 2, 699 (1957)].
[d] K. R. Lyall and J. F. Cochran, Can. J. Phys. 49, 1075 (1971).
[e] S. Haussuhl, Acta Crystallogr. A 24, 697 (1968).
[f] K. S. Aleksandrov and T. V. Ryzhova, Kristallografiya 6, 289 (1961) [Sov. Phys.-Crystallogr. 6, 228 (1961)].
[g] K. S. Aleksandrov, T. V. Ryzhova, and A. I. Rostuntseva, Kristallografiya 7, 930 (1962) [Sov. Phys.-Crystallogr. 7, 753 (1963)].
[h] R. K. Verma, J. Geophys. Res. 65, 757 (1960).
[i] W. R. Cook, Jr. and H. Jaffe, Acta Crystallogr. 10, 705 (1957).
[j] V. A. Koptsik, Kristallografiya 4, 219 (1959) [Sov. Phys.-Crystallogr. 4, 197 (1960)].
[k] R. V. G. Sundara Rao, Proc. Indian Acad. Sci. A 30, 173 (1949).
[l] R. F. S. Hearmon, Adv. Phys. 5, 323 (1956).
[m] J. Bhimasenachar and G. Venkata Rao, J. Acoust. Soc. Am. 29, 343 (1957).
[n] S. Haussuhl, Z. Naturforsch. A 24, 865 (1969).
[o] M. Silvestra, K. S. Aleksandrov, and A. A. Chumakov, Kristallografiya 3, 386 (1958) [Sov. Phys.-Crystallogr. 3, 388 (1958)].
[p] R. F. S. Hearmon, Rev. Mod. Phys. 18, 409 (1946).
[q] E. S. Fisher and D. Dever, Phys. Rev. 170, 607 (1968).

direction for an infinitesimal solid angle is

$$A = \Delta\Omega_k / \Delta\Omega_v . \tag{37}$$

The area of the group-velocity space for phonons arriving at the detector subtending an angle $\Delta\theta_v$ about the collinear axis is given by

$$\Delta\Omega_v = \pi(\Delta\theta_v)^2 . \tag{38}$$

In an orthorhombic material, for a circular group-velocity space, the wave-vector space for a cusp-free surface is nearly elliptical and its area is

$$\Delta\Omega_k = \pi(\Delta\theta_k)_a(\Delta\theta_k)_b . \tag{39}$$

The subscripts a and b refer to mutually orthogonal symmetry planes,[36] and $(\Delta\theta_k)_a$, $(\Delta\theta_k)_b$ are the angles subtended by the quasiellipse's semimajor and semiminor axes, respectively. The width of the wave-vector space in a symmetry plane which corresponds to $\Delta\theta_v$ is given by

$$(\Delta\theta_k)_a = (d\theta_k/d\theta_v)_a \Delta\theta_v \tag{40}$$

or

$$(\Delta\theta_k)_b = (d\theta_k/d\theta_v)_b \Delta\theta_v \ . \tag{41}$$

When the arrival points of the phonons on the detector surface lie within a circle, the amplification factor can be written

$$A(\theta_k, \phi_k) = \frac{\Delta\Omega_k}{\Delta\Omega_v} = \frac{\pi(d\theta_k/d\theta_v)_a \Delta\theta_v (d\theta_k/d\theta_v)_b \Delta\theta_v}{\pi(\Delta\theta_v)^2} ,$$

which simplifies to

$$A(\theta_k, \phi_k) = (d\theta_k/d\theta_v)_a (d\theta_k/d\theta_v)_b \ . \tag{42}$$

Numerically it is more convenient, however, to use a circular wave-vector space

$$\Delta\Omega_k = \pi(\Delta\theta_k)^2 \tag{43}$$

and calculate the corresponding group-velocity space $\Delta\Omega_v$. This is far more efficient in computer time than trying to calculate the wave-vector space for a circular group-velocity space where a binary search technique would have to be used for each point on the boundary of the surface. Examples of some calculated group-velocity spaces are plotted in Figs. 5 and 6 for a 1° departure from the collinear axis and 2° increments in the azimuthal angle measured from a reference symmetry plane. As the figures indicate, most of these spaces are nearly ellipses which subtend solid angles given by

$$\Delta\Omega_v = \pi(\Delta\theta_v)_a (\Delta\theta_v)_b \ . \tag{44}$$

For an infinitesimal detector the resulting expression for the PAF is independent of whether $\Delta\Omega_v$ or, conversely, $\Delta\Omega_k$ is chosen circular and, in fact, is really independent of the exact shape of the solid angle.

Selection of the appropriate phase-velocity surfaces in the mutually orthogonal symmetry planes is important. Figure 1 shows that the T_1 surface in the (100) symmetry plane meets the T_2 surface in the (010) symmetry plane along the [001] direction where $\rho s^2 = C_{55}$. To determine the PAF in the [001] direction for the $\rho s^2 = C_{55}$ surface, one must multiply the $(d\theta_k/d\theta_v)_a$ of the T_2 mode in the (010) plane by the $(d\theta_k/d\theta_v)_b$ of the T_1 mode in the (100) plane.

The [001] direction for the tetragonal and the ⟨100⟩ directions for the cubic lattice have two sets of orthogonal symmetry planes so that the PAF defined in the above manner for transverse waves does not have a unique value. In fact, since the transverse surfaces involved are neither circles nor ellipses (see Fig. 7), this condition is irrelevant. In this case, the area can be determined by numerical integration, which yields results that are in close agreement with those calculated from the averages of explicit expressions to be given in Table V.

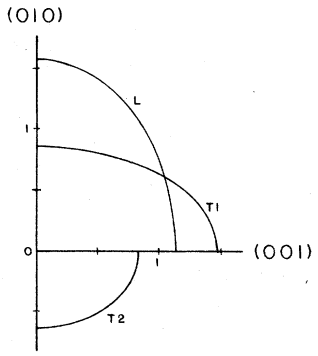

FIG. 5. Group-velocity directions which correspond to a quarter-circle of wave vectors located one degree from the [100] axis in gallium. For the counterclockwise rotation of the wave vector, the L and T_1 vectors rotate counterclockwise. The T_2 vector rotates clockwise because of the cusp about the [100] axis in the (001) plane. The origin is the [100] axis and the x and y axes are the (001) and (010) symmetry planes, respectively.

Along the η axis the derivative $d\theta_k/d\theta_v$ for the T_1 mode is given as follows:

$$\left.\frac{d\theta_k}{d\theta_v}\right|_{\theta_k=\theta_v=0} = \frac{a_2}{a_1} . \tag{45}$$

For the other two modes it is

$$\left.\frac{d\theta_k}{d\theta_v}\right|_{\theta_k=\theta_v=0} = \frac{a_4 \pm |a_6|}{a_3 \pm (2a_7^2 - a_5 a_6)/|a_6|} \tag{46}$$

where the "+" sign is used for the fast mode, the "−" sign for the slow mode, and the magnitude bars on a_6 for the case when $a_6 < 0$. In symmetry planes in directions perpendicular to the η axis the results are the same, but with a_1 and a_2 interchanged, a_3 and a_4 interchanged, and a_5 and a_6 interchanged.

Along the collinear axis θ_s, for the slow mode[37]

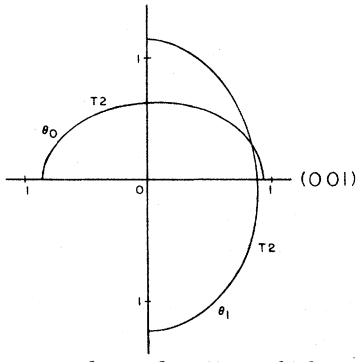

FIG. 6. Group-velocity directions which correspond to a semicircle of wave vectors located 1° from the θ_0 and the θ_1 axis in the (001) plane of gallium. For wave vectors around θ_0, the origin is the [100] axis and the x and y axes are the (001) and (010) symmetry planes, respectively. For wave vectors around θ_1, the origin is the [010] axis and the x and y axes are the (001) and (100) symmetry planes, respectively. Both vectors rotate counterclockwise.

$$\left.\frac{d\theta_k}{d\theta_v}\right|_{\theta_k=\theta_v=\theta_s} = \left(1 - \frac{4(a_6+|a_7|)(a_5+|a_7|)(a_5a_6-a_7^2)}{|a_7|[(a_5+|a_7|)+(a_6+|a_7|)][\frac{1}{2}(a_4+a_6)(a_5-a_6)+(a_4-|a_7|)(a_6+|a_7|)]}\right)^{-1} \tag{47}$$

and along the collinear axis θ_f, for the fast mode the same expression applies, but the signs preceding each $|a_7|$ are interchanged.[38] This result can be rewritten as

$$\left.\frac{d\theta_k}{d\theta_v}\right|_{\theta_k=\theta_v=\theta_f} = \left(1 - \frac{4(|a_7|-a_6)(|a_7|-a_5)(a_7^2-a_5a_6)}{|a_7|[(|a_7|-a_5)+(|a_7|-a_6)][\frac{1}{2}(a_4+a_6)(a_6-a_5)+(|a_7|+a_4)(|a_7|-a_6)]}\right)^{-1}. \tag{48}$$

Explicit expressions for the approximate PAF for orthorhombic, tetragonal, and cubic lattices are given in Tables III–V. Expressions for some directions have been omitted in the tetragonal and cubic tables since these are easily obtained from the orthorhombic and tetragonal expressions, respectively.

Consider now the phonon-amplification factor along the collinear axes in one symmetry plane only, for cusp-free group-velocity surfaces. Consider also a circular phonon detector, a distance D from a phonon source, centered about the collinear axis with its boundaries at an angle $\Delta\theta_v$ of approximately 1° from the collinear axis. The wave vectors which give rise to the phonons that strike the circular detector are found to lie in a solid angle which is almost elliptical (see Fig. 8). If a and b are the lengths of the semimajor and semiminor axes, respectively, of the quasiellipse surrounding the collinear direction, the PAF can be written

$$A = \Delta\Omega_k/\Delta\Omega_v = \pi ab/\pi(D\Delta\theta_v)^2 .$$

Furthermore, if the distance D from the phonon source to the detector is unity,

$$A = ab/(\Delta\theta_v)^2 . \tag{49}$$

When b lies in a symmetry plane which contains the [001] axis and the PAF along θ_2 is being considered, then

$$b = \Delta\theta_k = \Delta\theta_v \left.\frac{d\theta_k}{d\theta_v}\right|_{\theta_v=\theta_k=\theta_2} \tag{50}$$

and the PAF becomes

$$A = \frac{a}{\Delta\theta_v}\left.\frac{d\theta_k}{d\theta_v}\right|_{\theta_v=\theta_k=\theta_2} . \tag{51}$$

The $d\theta_k/d\theta_v$ factor was given in Eq. (47), but the factor $a/\Delta\theta_v$ is most easily determined numerically and is the same regardless of whether the solid angle, $\Delta\Omega_k$ or $\Delta\Omega_v$, is chosen circular. If a circular wave-vector space is chosen, the factor $a/\Delta\theta_v$ is the ratio of the radius of the wave-vector surface surrounding $\theta_k = \theta_s$ to a semiaxis of the quasiellipse (see Fig. 8) surrounding the collinear axis.

The PAF along the collinear axis θ_f can be found in an analogous manner.

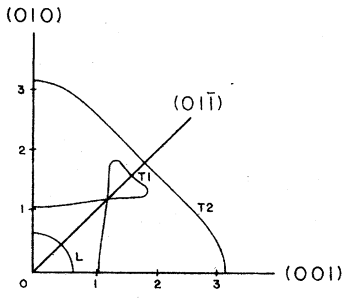

FIG. 7. Group-velocity directions which correspond to a quarter-circle of wave vectors located 1° from the [100] axis in cubic calcium fluoride. Note that the surfaces for the transverse modes are neither circles nor ellipses. Note also the cusp about the $(01\bar{1})$ plane in the T_1 mode where three different wave vectors give rise to the same group-velocity direction. For wave vectors rotated counterclockwise about the [100] axis, the group-velocity vectors all rotate counterclockwise. The origin is the [100] axis and the x and y axes are the (001) and (010) symmetry planes, respectively.

D. Conditions for cuspidal edges in symmetry planes

A cuspidal edge exists for wave vectors in a symmetry plane if $d\theta_k/d\theta_v < 0$. As a result, more than one wave-vector direction in a symmetry plane can give a group-velocity vector along one given direction (see Figs. 3 and 4). Cuspidal edges are always absent in the transverse T_1 mode and in the fast mode. This property is stated as Theorem III and proved in the Appendix.

Conditions for cuspidal edges in the slow mode about the various collinear axes in symmetry planes are as follows:

about the η axis:

$$a_7^2 > a_6(a_3+a_5)/2 \quad \text{if} \quad a_6 > 0, \tag{52}$$

but

$$a_7^2 > |a_6|(a_3-a_5)/2 \quad \text{if} \quad a_6 < 0; \tag{53}$$

about the $\eta_\perp$ axis:

$$a_7^2 > a_5(a_4+a_6)/2 \quad \text{if} \quad a_5 > 0, \tag{54}$$

but

$$a_7^2 > |a_5|(a_4-a_6)/2 \quad \text{if} \quad a_5 < 0; \tag{55}$$

TABLE III. Expressions for the phonon-amplification factor for orthorhombic lattices.

Axis	Surface	Amplification factor
[100]	$\rho S^2 = C_{66}$	$\left(\frac{C_{66}}{C_{44}}\right)\left(\frac{C_{66}}{C_{22}-(C_{12}+C_{66})^2/(C_{11}-C_{66})}\right)$
[100]	$\rho S^2 = C_{55}$	$\left(\frac{C_{55}}{C_{44}}\right)\left(\frac{C_{55}}{C_{33}-(C_{13}+C_{55})^2/(C_{11}-C_{55})}\right)$
[100]	$\rho S^2 = C_{11}$	$\left(\frac{C_{11}}{C_{55}+(C_{13}+C_{55})^2/(C_{11}-C_{55})}\right)\left(\frac{C_{11}}{C_{66}+(C_{12}+C_{66})^2/(C_{11}-C_{66})}\right)$
[010]	$\rho S^2 = C_{66}$	$\left(\frac{C_{66}}{C_{55}}\right)\left(\frac{C_{66}}{C_{11}-(C_{12}+C_{66})^2/(C_{22}-C_{66})}\right)$
[010]	$\rho S^2 = C_{44}$	$\left(\frac{C_{44}}{C_{55}}\right)\left(\frac{C_{44}}{C_{33}-(C_{23}+C_{44})^2/(C_{22}-C_{44})}\right)$
[010]	$\rho S^2 = C_{22}$	$\left(\frac{C_{22}}{C_{44}+(C_{23}+C_{44})^2/(C_{22}-C_{44})}\right)\left(\frac{C_{22}}{C_{66}+(C_{12}+C_{66})^2/(C_{22}-C_{66})}\right)$
[001]	$\rho S^2 = C_{55}$	$\left(\frac{C_{55}}{C_{66}}\right)\left(\frac{C_{55}}{C_{11}-(C_{13}+C_{55})^2/(C_{33}-C_{55})}\right)$
[001]	$\rho S^2 = C_{44}$	$\left(\frac{C_{44}}{C_{66}}\right)\left(\frac{C_{44}}{C_{22}-(C_{23}+C_{44})^2/(C_{33}-C_{44})}\right)$
[001]	$\rho S^2 = C_{33}$	$\left(\frac{C_{33}}{C_{55}+(C_{13}+C_{55})^2/(C_{33}-C_{55})}\right)\left(\frac{C_{33}}{C_{44}+(C_{23}+C_{44})^2/(C_{33}-C_{44})}\right)$

and about the θ_s axis:

$$4(a_6+|a_7|)(a_5+|a_7|)(a_5a_6-a_7^2) > |a_7|[(a_5+|a_7|)+(a_6+|a_7|)] \times [\tfrac{1}{2}(a_4+a_6)(a_5-a_6)+(a_4-|a_7|)(a_6+|a_7|)]. \quad (56)$$

Inequalities (52) and (54) have previously been derived by Musgrave[11] by considering the inverse phase-velocity surface. Inequality (56) follows from Theorem II in the Appendix.

If a cuspidal edge occurs in the slow mode about the η axis, wave vectors at angle θ_0 can also give group-velocity vectors parallel to the η axis where θ_0 is defined by

$$\tan^2\theta_0 = \frac{a_5a_6-2a_7^2}{a_5^2} \pm \frac{2a_3a_7}{a_5^2}\left(\frac{a_7^2-a_5a_6}{a_3^2-a_5^2}\right)^{1/2}, \quad (57)$$

where the choice in sign must make $\tan^2\theta_0$ positive. Similarly, a cuspidal edge about $\eta_\perp$ gives wave vectors at angle θ_1 with group-velocity vectors along $\eta_\perp$ where $\cot^2\theta_1$ replaces $\tan^2\theta_0$, a_4 replaces a_3, and a_5 is interchanged with a_6 in Eq. (57).

If, however, a cuspidal edge occurs about the collinear axis θ_s, solving for the other values of θ_k giving $\theta_v = \theta_s$ results in a sixth-degree equation in $\tan\theta_k$. This equation is identical for the fast and slow modes and has no general algebraic solution unless $a_3 = a_4$ and $a_5 = a_6$ as, for example, in the tetragonal lattice. In this case the [100] and [010] directions are equivalent and the collinear axis for the fast and slow modes is the [110] direction. Because of the symmetry, the equation can be factorized into three quadratic equations:

$$\tan^2\theta_k - 2\tan\theta_k + 1 = 0 \quad (58)$$

and

$$\tan^2\theta_k - 2(a \mp b)\tan\theta_k + 1 = 0, \quad (59)$$

where

$$a \mp b = -\left(\frac{a_7^2-a_5^2}{a_3^2-a_5^2}\right) \pm \frac{a_3}{a_5}\frac{[(a_7^2-a_5^2)(a_7^2-a_3^2)]^{1/2}}{a_3^2-a_5^2}, \quad (60)$$

giving two pairs of reciprocal roots:

$$\tan\theta_{3,4} = (a-b) \pm [(a-b)^2-1]^{1/2} \quad (61)$$

or

$$(a+b) \pm [(a+b)^2-1]^{1/2}. \quad (62)$$

Of course, one pair of these roots will be an extraneous complex conjugate pair for whichever sign gives $(a \mp b) < 1$.

In general, however, the sixth-degree equation cannot be factored. Although one root, $\tan\theta_s$, can be extracted, the resulting fifth-degree equation has no general algebraic solution and one of the

TABLE IV. Expression for the phonon-amplification factor for tetragonal lattices. For the [001] direction the two pairs of symmetry planes yield two different values whose average is the desired result.

Axis	Surface	Amplification factor	
[110]	$\rho S^2 = C_{44}$	$\left(\frac{C_{44}}{C_{33} - (C_{13}+C_{44})^2/[\frac{1}{2}(C_{11}+C_{12})+C_{66}-C_{44}]}\right)$	
[110]	$\rho S^2 = \frac{1}{2}(C_{11}-C_{12})$	$\left(\frac{\frac{1}{2}(C_{11}-C_{12})}{C_{44}}\right)\left(\frac{\frac{1}{2}(C_{11}-C_{12})}{\frac{1}{2}(C_{11}+C_{12})+C_{66}-(C_{11}-C_{66})^2/(C_{12}+C_{66})}\right)$	
[110]	$\rho S^2 = \frac{1}{2}(C_{11}+C_{12})+C_{66}$	$\left(\frac{\frac{1}{2}(C_{11}+C_{12})+C_{66}}{C_{44}+(C_{13}+C_{44})^2/[\frac{1}{2}(C_{11}+C_{12})+C_{66}-C_{44}]}\right)\left(\frac{\frac{1}{2}(C_{11}+C_{12})+C_{66}}{\frac{1}{2}(C_{11}-C_{12})+(C_{11}-C_{66})^2/(C_{12}+C_{66})}\right)$	
		$\phi = 0$, 90° planes	$\phi = -45$, 45° planes
[001]	$\rho S^2 = C_{44}$ (T_1)	$\left(\frac{C_{44}}{C_{66}}\right)^2$	$\left(\frac{2C_{44}}{C_{11}-C_{12}}\right)^2$
[001]	$\rho S^2 = C_{44}$ (T_2)	$\left(\frac{C_{44}}{C_{11}-(C_{13}+C_{44})^2/(C_{33}-C_{44})}\right)^2$	$\left(\frac{C_{44}}{\frac{1}{2}(C_{11}+C_{12})+C_{66}-(C_{13}+C_{44})^2/(C_{33}-C_{44})}\right)^2$
[001]	$\rho S^2 = C_{33}$	$\left(\frac{C_{33}}{C_{44}+(C_{13}+C_{44})^2/(C_{33}-C_{44})}\right)^2$	$\left(\frac{C_{33}}{C_{44}+(C_{13}+C_{44})^2/(C_{33}-C_{44})}\right)^2$

TABLE V. Expressions for the phonon-amplification factor for cubic lattices. As in the tetragonal case, when there are two values, their average yields a result which agrees within several percent with that obtained by numerical integration.

Axis	Surface	Amplification factor $\phi=0$, 90° planes	Amplification factor $\phi=-45$, 45° planes
⟨100⟩	$\rho S^2=C_{44}$ (T_1)	1	$\left(\frac{2C_{44}}{C_{11}-C_{12}}\right)^2$
⟨100⟩	$\rho S^2=C_{44}$ (T_2)	$\left(\frac{C_{44}}{C_{11}-(C_{12}+C_{44})^2/(C_{11}-C_{44})}\right)^2$	$\left(\frac{C_{44}}{\frac{1}{2}(C_{11}+C_{12})+C_{44}-(C_{12}+C_{44})^2/(C_{11}-C_{44})}\right)^2$
⟨100⟩	$\rho S^2=C_{11}$ (L)	$\left(\frac{C_{11}}{C_{44}+(C_{12}+C_{44})^2/(C_{11}-C_{44})}\right)^2$	$\left(\frac{C_{11}}{C_{44}+(C_{12}+C_{44})^2/(C_{11}-C_{44})}\right)^2$
⟨111⟩	$\rho S^2=\frac{1}{3}(C_{11}+4C_{44}+2C_{12})$ (L)		$\left(1+\frac{4wx}{(C_{12}+C_{44})yz}\right)^{-2}$

$w=[C_{11}-C_{44}-(C_{12}+C_{44})][\frac{1}{2}(C_{11}+C_{12})-(C_{12}+C_{44})]$,

$x=\frac{1}{2}(C_{11}+C_{12})(C_{11}-C_{44})-(C_{12}+C_{44})^2$,

$y=\frac{1}{2}(C_{11}+C_{12})+C_{11}-C_{44}-2(C_{12}+C_{44})$,

and

$z=C_{11}C_{44}+\frac{1}{2}C_{11}(C_{11}+C_{12})-C_{44}^2-2C_{44}(C_{12}+C_{44})-(C_{12}+C_{44})^2$

remaining roots must be obtained numerically. It is most convenient to numerically determine a root, $\tan\theta_5$, corresponding to $\theta_v=\theta_s$ for the fast mode. The resulting quartic equation can be factored using the method of Descartes or Ferrari,[39] giving a pair of positive real roots, $\tan\theta_3$ and $\tan\theta_4$, respectively, and a pair of complex conjugate roots. Such a solution has been performed for a number of crystals and the results are listed in Tables VI–VIII.

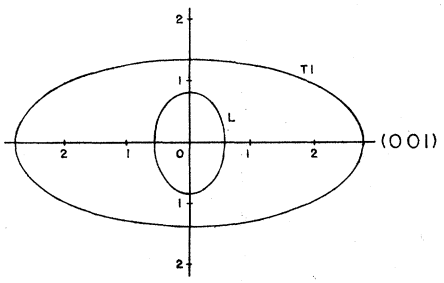

FIG. 8. Group-velocity directions which correspond to circles of wave vectors located 1° from the θ_2 and the θ_6 cusp-free collinear axes in the (001) plane of orthorhombic gallium. The larger ellipse surrounds θ_2; the smaller is around θ_6. The y axis is an orthogonal nonsymmetry plane. Both rotations are counterclockwise.

E. Conditions for phonon focusing in symmetry planes about collinear, cusp-free axes

A symmetry plane is cusp free if $d\theta_k/d\theta_v>0$ and exhibits cusp-free phonon focusing if $d\theta_k/d\theta_v>1$. Cusp-free phonon focusing thus occurs for wave vectors in a symmetry plane about a collinear axis if $(d\theta_k/d\theta_v)_{\theta_k=\theta_v}>1$.

Conditions for cusp-free phonon focusing along η for each mode are as follows:

fast mode: $a_6^2>a_7^2$ if $a_6>0$, (63)

but $a_5a_6>a_7^2$ if $a_6<0$; (64)

slow mode: $a_7^2>a_5a_6$ if $a_6>0$, (65)

but $a_7^2>a_6^2$ if $a_6<0$; (66)

T_1 mode: $a_2>a_1$. (67)

Similarly, conditions for cusp-free focusing along $\eta_\perp$ are as follows:

fast mode: $a_5^2>a_7^2$ if $a_5>0$, (68)

but $a_5a_6>a_7^2$ if $a_5<0$; (69)

slow mode: $a_7^2>a_5a_6$ if $a_5>0$, (70)

but $a_7^2>a_5^2$ if $a_5<0$; (71)

T_1 mode: $a_1>a_2$ (72)

For cusp-free focusing of the fast mode along θ_f:

$a_7^2>a_5a_6$, (73)

TABLE VI. Collinear axes and other directions associated with cusps in symmetry planes of orthorhombic crystals. The angles θ_i, which are defined as in Figs. 3 and 4, are measured in degrees. In the (010) and (100) planes, entries under θ_0 and θ_1 indicate cuspidal edges about directions parallel and perpendicular, respectively, to the [001] axis. In the (001) plane, entries under θ_0 and θ_1 indicate cuspidal edges about the [100] and [010] directions, respectively. In the (010) and (100) planes, entries under θ_3 and θ_4 indicate cuspidal edges about directions having an angle θ_2 with respect to the [001] axis. In the (001) plane, entries under θ_3 and θ_4 indicate cuspidal edges about directions having an angle θ_2 with respect to the [100] axis.

Orthorhombic material	(010), (100), and (001) planes, respectively					
	θ_0	θ_1	θ_2	θ_3	θ_4	θ_6
Aragonite	•••	•••	36.18	7.28	65.81	28.62
	•••	•••	44.66	•••	•••	47.80
	•••	•••	51.54	•••	•••	•••
Barium sulphate	•••	•••	47.42	•••	•••	•••
	•••	•••	46.76	10.77	81.86	50.96
	22.06	68.74	44.44	•••	•••	49.36
Benzophenone	•••	•••	40.11	8.55	72.44	32.01
	•••	•••	41.46	•••	•••	•••
	19.46	69.39	45.63	•••	•••	40.44
Gallium (at 4.2 °K)	•••	•••	48.27	•••	•••	•••
	•••	•••	49.72	•••	•••	•••
	22.68	66.50	46.16	•••	•••	39.69
Iodic acid	25.07	64.90	48.83	•••	•••	33.17
	•••	•••	41.26	•••	•••	14.80
	16.19	•••	38.28	•••	•••	•••
Iodic acid	24.97	64.96	48.85	•••	•••	33.14
(deuterated)	•••	•••	41.26	•••	•••	13.70
	16.50	•••	38.28	•••	•••	•••
Lithium ammonium	•••	•••	44.29	12.34	76.28	42.85
tartrate	•••	•••	41.12	•••	•••	•••
monohydrate	24.60	66.50	41.50	•••	•••	58.50
Magnesium sulphate	32.74	57.00	44.71	•••	•••	45.82
heptahydrate	•••	80.38	45.80	•••	•••	34.15
	10.99	73.83	46.10	•••	•••	33.54
Nickel sulphate	33.52	53.99	44.53	•••	•••	46.28
heptahydrate	21.03	67.95	45.66	•••	•••	39.23
	20.18	67.99	46.14	•••	•••	35.42
Olivine	•••	•••	42.06	•••	•••	17.25
	•••	•••	47.43	•••	•••	•••
	•••	•••	50.68	•••	•••	•••
Potassium	•••	•••	36.99	5.82	68.57	•••
pentaborate	37.37	48.23	42.23	•••	•••	51.10
	•••	•••	49.59	19.38	80.76	75.49
Resorcinol	33.17	58.36	46.96	•••	•••	36.79
	•••	•••	43.95	•••	•••	•••
	17.63	•••	41.83	•••	•••	•••
Rochelle salt	•••	•••	48.87	11.47	84.22	•••
	•••	•••	46.91	•••	•••	•••
	•••	•••	42.73	•••	•••	•••
Sodium ammonium	•••	•••	48.47	13.44	82.67	•••
tartrate	•••	•••	45.73	•••	•••	17.55
	•••	•••	42.15	•••	•••	•••

TABLE VI. (*Continued*)

Orthorhombic material	(010), (100), and (001) planes, respectively θ_0	θ_1	θ_2	θ_3	θ_4	θ_6
Sodium tartrate	...	...	48.32	7.51	85.80	62.15
	...	...	46.77	...	...	...
	...	...	43.44	...	...	...
Staurolite	...	...	35.66	...	...	...
	34.32	53.65	43.15	...	...	55.30
	...	...	51.90	...	...	...
Strontium sulphate	...	...	46.96	...	...	...
	...	...	46.80	14.99	78.83	56.65
	30.63	59.31	44.87	...	...	45.96
Sulfur	...	...	48.02	27.79	71.47	58.29
	34.18	59.00	48.44	...	...	35.90
	...	...	46.34	...	...	58.30
Terpine monohydrate	...	...	47.00	20.49	74.90	57.80
	...	...	49.65	25.71	77.00	68.94
	...	...	47.49	...	...	...
Topaz	6.98	79.41	45.50	...	...	41.92
	...	...	43.07	...	...	...
	19.50	76.07	42.79	...	...	58.88
Uranium (at 4.2 °K)	...	75.30	55.72	...	...	...
	32.23	60.06	47.97	...	...	37.44
	20.68	...	37.67	...	...	...
Zinc sulphate heptahydrate	33.89	55.77	44.67	...	...	45.96
	18.08	70.05	45.77	...	...	36.74
	...	...	46.15	...	...	20.06

and for the slow mode along θ_s:

$$a_5 a_6 > a_7^2. \tag{74}$$

Inequalities (73) and (74) follow from Theorems I and II, respectively, in the Appendix.

F. Phonon-amplification factor for the orthorhombic lattice when cuspidal edges are present

The presence of a cuspidal edge increases the phonon-amplification factor because wave vectors in more than one direction contribute to group-velocity vectors in a given direction. Consider a circular phonon detector centered about the [001] axis with its boundaries at an angle $\Delta\theta_v$ of approximately 1° from this axis. If a cusp exists along the [001] axis, there are additional wave-vector spaces besides the one about the [001] axis which provide phonons that strike the detector. Orthorhombic uranium, for example, has a cusp about the [001] axis in the (100) plane, (see Table VI), so that two wave-vector spaces near $\theta_k = \theta_0 = 32.23°$, one on each side of the [001] axis in the (100) plane, give rise to phonons that strike a phonon detector centered about the [001] axis. In orthorhombic topaz, for example, there are two cuspidal edges about the [100] axis, one in the (001) plane, the other in the (010) plane, (see Table VI). If a circular phonon detector is centered about the [100] axis, wave vectors near the [100] axis, the two θ_0 directions (one on each side of the [100] axis in the (001) plane), and the two θ_1 directions (one on each side of the [100] axis in the (010) plane) give rise to transversely polarized phonons which strike the detector. The two cusps, however, occur on different velocity surfaces (see Fig. 1) so that each transverse velocity surface has contributions from only two wave-vector spaces in addition to the one about the [100] axis. A similar situation exists about the [010] axis. If a circular detector is centered about a θ_2 collinear axis about which there is a cusp, then wave-vector spaces surrounding θ_2, θ_3, and θ_4 give rise to phonons that strike the detector (see Fig. 3).

If the solid angle $\Delta\Omega_v$ subtended by the detector is circular, the wave-vector solid angles $\Delta\Omega_k$ surrounding the collinear axes or the θ_0, θ_1, θ_3, and θ_4 directions are nearly elliptical. Let a and b be the lengths of the semimajor and semiminor axes, respectively, of the quasiellipse surrounding the collinear direction, and let a_i and b_i be the lengths of the semimajor and semiminor axes of a quasiellipse about either the θ_0 or θ_1 directions. Since there are three wave-vector spaces contributing

TABLE VII. Collinear axes and other directions associated with cusps in symmetry planes of tetragonal crystals. The angles θ_i which are defined as in Figs. 3 and 4, are measured in degrees. In the (010) and (110) planes, entries under θ_0 and θ_1 indicate cuspidal edges about directions parallel and perpendicular, respectively, to the [001] axis. In the (001) plane, entries under θ_0 and θ_1 indicate cuspidal edges about the [100] and [010] directions, respectively. In the (010) and (110) planes, entries under θ_3 and θ_4 indicate cuspidal edges about directions having an angle θ_2 with respect to the [001] axis. In the (001) plane, entries under θ_3 and θ_4 indicate cuspidal edges about directions having an angle θ_2 with respect to the [100] axis.

Tetragonal material	(010), (110), and (001) planes, respectively θ_0	θ_1	θ_2	θ_3	θ_4	θ_6
Ammonium dihydrogen	···	···	37.69	10.40	59.02	···
phosphate	···	···	42.76	···	···	···
	···	···	45.00	5.05	84.95	45.00
Indium (at 4.2 °K)	32.98	56.78	44.66	···	···	48.98
	13.72	···	43.39	···	···	···
	33.42	56.58	45.00	···	···	45.00
Indium bismuth	36.51	48.67	41.48	···	···	53.34
	33.53	50.54	40.40	···	···	60.70
	33.73	56.27	45.00	···	···	45.00
Nickel sulphate	···	···	43.78	···	···	37.49
hexahydrate	···	···	39.11	16.51	55.40	24.04
	38.63	51.37	45.00	···	···	45.00
Paratellurite	···	···	52.07	···	···	···
	···	···	43.56	16.52	69.77	39.83
	43.91	46.09	45.00	···	···	45.00
Potassium dihydrogen	···	···	44.12	18.25	69.23	39.92
phosphate	···	···	47.58	···	···	···
	···	···	45.00	5.53	84.47	45.00
Rutile	···	85.07	50.83	···	···	···
	···	···	46.54	···	···	62.02
	38.24	51.76	45.00	···	···	45.00
White tin	···	···	47.30	···	···	···
(at 4.2 °K)	···	···	45.49	···	···	50.26
	33.65	56.35	45.00	···	···	45.00
Zircon	···	···	39.60	13.77	60.76	21.08
	···	···	42.53	25.59	55.10	28.67
	···	···	45.00	14.66	75.34	45.00
Zirconium silicate	···	···	46.57	35.06	61.15	57.22
	···	···	50.17	···	···	···
	···	···	45.00	7.18	82.82	45.00

phonons which strike the detector, (the distance D from the source of phonons to the detector is assumed to be unity), the PAF can be written as

$$A=\frac{\sum\Delta\Omega_k}{\Delta\Omega_v}=\frac{\pi ab+2\pi a_i b_i}{\pi(D\Delta\theta_v)^2}=\frac{ab+2a_i b_i}{(\Delta\theta_v)^2}. \tag{75}$$

For example, if the PAF along the [001] axis in uranium is considered, then additional contributing wave-vector spaces surround θ_0 in the (100) plane. Since a is evaluated for the T_1 portion, and b for the T_2 portion of the surface $\rho s^2=C_{44}$ (see Fig. 1),

$$a=\Delta\theta_k\big|_{\theta_k=0}=\Delta\theta_v\left|\frac{d\theta_k}{d\theta_v}\right|_{\theta_k=\theta_v=0}=\Delta\theta_v\left(\frac{a_2}{a_1}\right), \tag{76}$$

$$b=\Delta\theta_k\big|_{\theta_k=0}=\Delta\theta_v\left|\frac{d\theta_k}{d\theta_v}\right|_{\theta_k=\theta_v=0}=\Delta\theta_v\left|\frac{a_4-|a_6|}{a_3-(2a_7^2-a_5a_6)/|a_6|}\right|, \tag{77}$$

TABLE VIII. Collinear axes and other directions associated with cusps in symmetry planes of cubic crystals. The entries are as described in Table VII.

Cubic material	(010) and (110) planes, respectively θ_0	θ_1	θ_2	θ_3	θ_4	θ_5
Calcium fluoride	···	···	45.00	19.22	70.78	45.00
	···	···	46.52	26.76	68.31	54.74
Diamond	···	···	45.00	···	···	45.00
	···	···	43.85	···	···	54.74
Lead (at 0 °K)	39.16	50.84	45.00	···	···	45.00
	33.12	55.07	43.10	···	···	54.74
Lithium fluoride	23.86	66.14	45.00	···	···	45.00
	18.73	75.81	43.09	···	···	54.74
Magnesium oxide	21.03	68.97	45.00	···	···	45.00
(at 4.2 °K)	15.50	82.41	43.28	···	···	54.74
Niobium (at 4.2 °K)	···	···	45.00	13.96	76.04	45.00
	···	···	46.07	19.19	73.80	54.74
Silicon	23.65	66.35	45.00	···	···	45.00
	18.15	76.58	43.32	···	···	54.74
Sodium fluoride	···	···	45.00	24.09	65.91	45.00
	···	···	46.59	33.82	62.17	54.74

$$b_i = b_0 = \Delta\theta_k\big|_{\theta_k=\theta_0} = \Delta\theta_v \left|\frac{d\theta_k}{d\theta_v}\right|_{\theta_k=\theta_0,\,\theta_v=0}, \tag{78}$$

$$\left.\frac{d\theta_k}{d\theta_v}\right|_{\theta_k=\theta_0,\,\theta_v=0} = \frac{2a_4a_7[(a_7^2-a_5a_6)/(a_3^2-a_5^2)]^{1/2}-[(2a_7^2-a_5a_6)\tan^2\theta_0+a_6^2]}{(2\tan^2\theta_0)(1+\tan^2\theta_0)(a_3^2-a_5^2)} \tag{79}$$

where $\tan^2\theta_0$ is given by Eq. (57).

Note that a in Eq. (76) is evaluated in the (010) plane, but that b and b_0 in Eqs. (77) and (79), respectively, are evaluated in the (100) plane. Since the cusp occurs about the [001] axis in the (100) plane, the value of $(ab)/(\Delta\theta_v)^2$ can be found by taking the magnitude of the expression for the PAF given in Table III for the $\rho s^2 = C_{44}$ surface along the [001] axis. The factor $a_0/\Delta\theta_v$ is most easily determined numerically and is the same if either solid angle, $\Delta\Omega_k$ or $\Delta\Omega_v$, is chosen circular. If a circular wave-vector space is chosen, then the factor $a_0/\Delta\theta_v$ is the ratio of the radius of the wave-vector surface surrounding $\theta_k = \theta_0$ to a semiaxis of the quasiellipse surrounding the collinear axis.

For a cusp about the [100] axis, for example in the (010) plane, the results are similar. Evaluating a for the T_1 portion, and b for the T_2 portion of the surface $\rho s^2 = C_{55}$ (see Fig. 1) yields results (76)–(79), but with $\cot^2\theta_1$ replacing $\tan^2\theta_0$, a_3 interchanged with a_4, and a_5 interchanged with a_6. Note again that a is evaluated in the (001) plane, but b and b_1 are evaluated in the (010) plane. Again, $(ab)/(\Delta\theta_v)^2$ can be found using the magnitude of the PAF given in Table III for the $\rho s^2 = C_{55}$ surface along the [100] axis.

For a cusp about the [100] axis in the (001) plane, a and b are evaluated for the $\rho s^2 = C_{66}$ surface giving results (76)–(79), but with a_1 and a_2 interchanged. In this case a is evaluated for the (010) plane, but b and b_1 are evaluated in the (001)

plane. A cusp about [010] in either the (100) plane or the (001) plane can be treated in a similar manner.

Since the collinear axis θ_2 is in general not at the intersection of orthogonal symmetry planes, the determination of the PAF is slightly different for a cusp about this axis. When a given θ_2 axis lies in only one symmetry plane, the quasielliptical wave-vector spaces around θ_3 and θ_4 are neither equal nor located at equal angular distances from θ_2.

The PAF for this case can be written, using the form of Eq. (75), as

$$A=\frac{\sum \Delta\Omega_k}{\Delta\Omega_v}=\frac{\pi ab+\pi a_3b_3+\pi a_4b_4}{\pi(D\Delta\theta_v)^2}=\frac{ab+a_3b_3+a_4b_4}{(\Delta\theta_v)^2}, \tag{80}$$

where

$$b=\Delta\theta_k\big|_{\theta_k=\theta_2}=\Delta\theta_v\left|\frac{d\theta_k}{d\theta_v}\right|_{\theta_k=\theta_v=\theta_2}, \tag{81}$$

which can be evaluated from Eq. (47),

$$b_3=\Delta\theta_k\big|_{\theta_k=\theta_3}=\Delta\theta_v\left|\frac{d\theta_k}{d\theta_v}\right|_{\theta_k=\theta_3,\ \theta_v=\theta_2}, \tag{82}$$

$$b_4=\Delta\theta_k\big|_{\theta_k=\theta_4}=\Delta\theta_v\left|\frac{d\theta_k}{d\theta_v}\right|_{\theta_k=\theta_4,\ \theta_v=\theta_2}. \tag{83}$$

When these values are substituted into Eq. (80), the PAF becomes

$$A=\frac{a_3}{\Delta\theta_v}\left|\frac{d\theta_k}{d\theta_v}\right|_{\theta_k=\theta_3,\ \theta_v=\theta_2}+\frac{a_4}{\Delta\theta_v}\left|\frac{d\theta_k}{d\theta_v}\right|_{\theta_k=\theta_4,\ \theta_v=\theta_2}$$
$$+\frac{a}{\Delta\theta_v}\left|\frac{d\theta_k}{d\theta_v}\right|_{\theta_k=\theta_v=\theta_2}. \tag{84}$$

The coefficient factors $a/\Delta\theta_v$, $a_3/\Delta\theta_v$, and $a_4/\Delta\theta_v$ can be determined numerically as before. Although the derivatives in Eqs. (82) and (83) can be represented by long expressions, they too are most easily calculated numerically.

For noncollinear directions, it is more convenient to use numerical integration to count the number of group-velocity vectors falling within a small solid angle using a fine angular mesh and a uniform angular density of k vectors. This has been done for some orthorhombic, tetragonal, and cubic crystals. The highest and lowest phonon intensities obtained along with their directions are listed in Tables IX and X. Phonon intensities obtained by the above method near collinear directions are given in Tables XI–XIII. More accurate calculations of phonon intensities using the dimensions of ellipses and circles are given in Table XIV.

In the [001] direction tetragonal and cubic materials have two sets of mutually orthogonal symmetry planes. For a circular phonon detector and group-velocity space centered on the [001] direction, the corresponding wave-vector space must have four-fold symmetry and thus can not be a quasiellipse. Conversely, the group-velocity space corresponding to a circular wave-vector space is not quasielliptic. The vector spaces for cubic calcium fluoride in Fig. 7 clearly illustrate this and even indicate the presence of a cusp. Numerical integration may be used to determine the area of the surface when such a cusp is present.

When a cusp exists about the [110] direction in tetragonal and cubic materials, circular wave vector spaces centered about the [110] direction, the θ_1 directions in the (110) plane, or the θ_3 and θ_4 directions in the (001) plane can be expected to give rise to quasielliptic group-velocity surfaces about the [110] direction. Calculation of the areas of the two group-velocity spaces which correspond to wave vectors about θ_3 and θ_4 is shortened by the fact that these areas are equal and located at equal angular distances from θ_2.

In cubic crystals no cusp is expected about the ⟨111⟩ directions because collinear axes exist in these directions only for the L mode. For a circular wave-vector space centered about the [111] direction the corresponding group-velocity space has three-fold symmetry. However, for 1° angular deviations about the ⟨111⟩ directions the resulting group-velocity space is very nearly circular and thus its approximate area can be easily calculated.

G. Effect of phonon focusing on phonon conduction

In the orthorhombic lattice the phase velocities along the x, y, and z axes are in general different so that the thermal conductivity can be expected to be anisotropic at all temperatures. In the boundary-scattering regime, where ballistic phonon propagation occurs, phonon focusing can be responsible for anisotropic heat conduction even when the phonon phase velocities along the x, y, and z axes are equal. In fact, focusing will always be present whenever a solid is elastically anisotropic and occurs even in cubic crystals.

TABLE IX. Calculated maximum and minimum phonon intensities in orthorhombic materials. The directions at which the extrema occur are given by the spherical polar angles θ and ϕ in degrees. The angle θ is measured with respect to the [001] axis and the angle ϕ is measured in the (001) plane with respect to the [100] axis. For an elastically isotropic solid the corresponding intensities are unity. Calculations were performed using a 1° mesh in θ and ϕ, the number of wave vectors at each point weighted to give a uniform density. Because of this mesh, a much larger number of different wave vector directions fell within a 1° deviation from the [001] axis than for any other axis making any azimuthal variation in intensity about the [001] axis clearly observable. This is indicated in the table.

Orthorhombic material	Highest phonon intensity	Direction θ	Direction ϕ	Lowest phonon intensity	Direction θ	Direction ϕ
Aragonite	23.80	90	90	0.00	52	90
Barium sulphate	43.39	90	04	0.00	90	44
Benzophenone	27.95	80	90	0.00	52	90
Gallium (at 4.2 °K)	16.89	48	60	0.00	40	90
Iodic acid	26.17	00	64	0.00	16	00
Lithium ammonium tartrate monohydrate	34.06	82	90	0.00	40	90
Magnesium sulphate heptahydrate	30.50	08	00	0.00	90	74
Nickel sulphate heptahydrate	35.62	00	34	0.00	62	60
Olivine	10.42	42	02	0.00	46	90
Potassium pentaborate	34.88	00	68	0.00	48	90
Resorcinol	32.62	00	30	0.00	90	70
Rochelle salt	7.31	72	40	0.00	90	00
Sodium tartrate	14.10	72	00	0.00	90	00
Staurolite	23.98	90	20	0.00	48	90
Strontium sulphate	40.33	90	12	0.00	90	56
Sulfur	33.95	00	68	0.00	28	68
Terpine monohydrate	9.00	00	74	0.00	24	00
Topaz	64.40	00	86	0.00	90	74
Uranium (at 4.2 °K)	32.77	80	90	0.00	44	44
Zinc sulphate heptahydrate	35.40	00	78	0.00	30	00

The anisotropy in the thermal conductivity of cubic crystals was first reported by McCurdy, Maris, and Elbaum[5] on measurements made in silicon and calcium fluoride. Anisotropies of up to 50% for silicon and 40% for calcium fluoride were observed and shown to be the direct result of phonon focusing arising from elastic anisotropy.

Phonon focusing and conductivity calculations have also been made by McCurdy for elastically anisotropic hexagonal crystals.[13] For materials having large elastic anisotropies differences in phonon intensity (up to factors of several hundred) were predicted for various crystallographic directions. Calculations of the thermal conductivity demonstrated that the phonon-focusing property could cause differences in the phonon conductivity in the ballistic regime by as much as 300%.

Winternheimer and McCurdy[14] have predicted that the phonon-focusing property will cause anisotropic heat conduction even in cubic superconductors providing the temperature is a small fraction of the superconducting transition temperature, and the phonon mean-free path approaches sample dimensions, (i.e., $\Lambda_{ph} \sim l$).

Calculations have been made for a number of

TABLE X. Calculated maximum and minimum phonon intensities in tetragonal and cubic materials. The corresponding intensities for an elastically isotropic solid are unity. The angles θ and ϕ are defined in Table IX. Calculations were performed using the same mesh as described in Table IX. The suffix L refers to the longitudinal mode.

Tetragonal material	Highest phonon intensity	Direction θ	Direction ϕ	Lowest phonon intensity	Direction θ	Direction ϕ
Ammonium dihydrogen phosphate	31.30L	88	00	0.00	90	00
Indium (at 4.2 °K)	11.34	74	12	0.00	24	45
Nickel sulphate hexahydrate	13.93	46	42	0.00	00	00
Paratellurite	64.32	00	30	0.00	90	00
Potassium dihydrogen phosphate	10.00L	90	00	0.00	90	00
Rutile	28.50	00	04	0.00	90	45
White tin (at 4.2 °K)	10.47	56	20	0.00	22	00
Zirconium silicate	14.61	46	00	0.00	90	00
Cubic material						
Calcium fluoride	9.49	88	38	0.00	90	00
Lead (at 0 °K)	32.65	28	00	0.00	46	45
Lithium fluoride	46.61	00	38	0.00	54	45
Magnesium oxide (at 4.2 °K)	51.62	00	44	0.00	54	45
Niobium (at 4.2 °K)	12.24	64	30	0.00	72	16
Silicon	34.65	04	04	0.00	54	45
Sodium fluoride	14.06	48	26	0.00	54	45

orthorhombic and tetragonal crystals, and, as expected, anisotropic phonon conductivity was predicted in those crystals which were elastically anisotropic. The direction of high thermal conductivity always coincided with the direction in which the PAF was high. To illustrate the effects of focusing, calculations were performed to determine the phonon-conduction-enhancement factor A_κ defined as

$$A_\kappa = \kappa_v/\kappa_s , \tag{85}$$

where κ_v is the thermal conductivity calculated by correctly including effects of phonon focusing and κ_s is the thermal conductivity calculated using phase-velocity vectors instead of group-velocity vectors for each mode. Calculations of κ_s thus disregard the angular deviation between the group-velocity vectors and their corresponding wave vectors for elastically anisotropic solids. Values of κ_s depend on the crystallographic direction of the heat-flow axis and will be largest in those directions having the largest inverse-square phase velocity averaged over the three modes.

Samples used in the calculation of κ_v and κ_s were assumed to have circular cross-sections with a thermal length of 3 cm and a diameter D of 0.3 cm. Calculations of the thermal conductivity κ_v; end-corrected mean free path, Λ_{corr}; and thermal-conduction-enhancement factors A_κ are given in Table XV for several crystallographic directions. For elastically isotropic solids the thermal-conductivity-enhancement factor A_κ is unity, and the end-corrected mean free path Λ_{corr} is $0.926D$. Note that higher values of thermal conductivity coincide with higher values of A_κ. Tables VI–XV show that the highest values of thermal conductivity are found along directions about which cuspidal edges exist. The above results should be applicable (for dielectric solids) at temperatures which are a small fraction of the Debye temperature. For the superconductors, however, these results should not apply until the temperature becomes a

TABLE XI. Approximate phonon-amplification factor $A(\theta_v, \phi_v)$ in some orthorhombic crystals near collinear directions. The PAF values given are those calculated at the nearest even integer number of degrees to the collinear axes. The PAF was calculated as the ratio of the number of group-velocity vectors to the number of wave vectors for a solid angle of 4 square degrees. Four wave vectors were used in each $2°\times2°$ box and each box was weighted to give a uniform density of wave vectors over all space. Entries for θ and ϕ are in degrees.

(θ_v, ϕ_v)		Aragonite	Barium sulphate	Benzophenone	Ga (at 4.2 °K)	Strontium sulphate	Topaz	U (at 4.2 °K)
(0, 0)	L	0.00	2.00	0.00	4.00	2.00	1.00	0.00
	Slow T	0.00	0.00	0.00	1.00	0.00	1.00	4.00
	Fast T	3.00	1.00	1.00	1.00	1.00	0.00	0.00
$(\theta_6, 0)$	L	0.51	···	0.00	···	···	1.51	···
	Slow T	1.38	···	2.95	···	···	1.03	···
	Fast T	0.68	···	1.31	···	···	0.90	···
	θ_6	28.62	···	32.01	···		41.92	···
$(\theta_2, 0)$	L	0.43	1.09	0.00	1.10	1.10	1.54	0.00
	Slow T	13.51	0.59	4.60	2.92	0.65	0.99	0.50
	Fast T	0.51	0.00	0.51	0.00	0.00	0.45	1.64
	θ_2	36.18	47.42	40.11	48.27	46.96	45.50	55.72
(90, 0)	L	9.99	1.00	4.00	1.00	1.00	0.00	0.00
	Slow T	0.00	13.95	0.00	5.00	6.00	14.91	3.96
	Fast T	1.00	2.00	12.00	2.00	2.00	3.00	0.00
$(90, \phi_6)$	L	···	3.00	4.50	2.00	2.00	1.50	···
	Slow T	···	1.50	0.00	0.00	0.00	0.50	···
	Fast T	···	0.00	0.50	0.00	0.00	1.00	···
	ϕ_6	···	49.36	40.44	39.69	45.96	58.88	···
$(90, \phi_2)$	L	1.00	3.00	4.50	2.00	1.50	1.50	0.00
	Slow T	4.48	2.50	0.00	0.00	0.50	0.50	0.50
	Fast T	0.00	0.00	0.50	0.00	0.00	1.00	2.43
	ϕ_2	51.54	44.44	45.63	46.16	44.87	42.79	37.67
(90, 90)	L	0.00	2.00	2.00	0.00	1.00	1.00	0.00
	Slow T	23.80	0.00	1.00	1.00	1.00	1.00	17.29
	Fast T	4.00	5.00	7.00	1.00	1.00	17.00	0.00
$(\theta_2, 90)$	L	0.98	0.52	0.84	0.56	1.06	0.46	6.12
	Slow T	3.49	1.52	3.00	1.03	4.66	1.51	0.00
	Fast T	0.00	0.00	0.00	0.00	2.49	9.66	0.97
	θ_2	44.66	46.76	41.46	49.72	46.80	43.07	47.97
$(\theta_6, 90)$	L	1.00	0.50	···	···	0.50	···	6.13
	Slow T	3.20	7.06	···	···	8.15	···	0.58
	Fast T	0.00	0.00	···	···	2.03	···	1.91
	θ_6	47.80	50.96	···	···	56.65	···	37.44
(θ_{ns}, ϕ_{ns}) [a]	L	1.00	1.25	···	1.50	1.25	···	···
	θ_{ns}	48.55	57.80	···	62.57	58.31	···	···
	ϕ_{ns}	85.18	28.47	···	35.83	33.84	···	···
(θ_{ns}, ϕ_{ns})	Slow T	···	···	···	0.97	2.20	3.30	···
	θ_{ns}	···	···	···	16.73	36.98	48.47	···
	ϕ_{ns}	···	···	···	31.81	31.35	67.16	···
(θ_{ns}, ϕ_{ns})	Fast T	···	3.26	···	12.08	10.19	0.50	0.00
	θ_{ns}	···	46.06	···	47.25	45.83	42.74	50.18
	ϕ_{ns}	···	47.14	···	43.42	44.47	56.84	41.13

[a] θ_{ns}, ϕ_{ns} are the nonsymmetry collinear axes.

TABLE XII. Approximate phonon-amplification factor in some tetragonal crystals. The entries are as described in Table XI.

(θ_v, ϕ_v)		In (at 4.2 °K)	Nickel sulphate hexahydrate	TeO_2 [a]	KDP [b]	Rutile	White tin (at 4.2 °K)	Zirconium silicate
(0, 0)	L	1.00	1.00	4.00	4.00	1.00	1.00	4.00
	Slow T	1.00	4.00	0.00	0.00	18.00	4.00	0.00
	Fast T	0.00	0.00	0.00	0.00	1.00	0.00	0.00
$(\theta_6, 0)$	L	1.49	0.49	···	2.00	···	···	3.00
	Slow T	0.00	0.00	···	0.00	···	···	0.00
	Fast T	2.13	0.00	···	4.92	···	···	1.13
	θ_6	48.98	37.49	···	39.92	···	···	57.22
$(\theta_2, 0)$	L	1.46	0.00	0.00	0.97	0.00	1.09	1.06
	Slow T	0.00	0.00	0.00	0.00	1.59	0.58	0.00
	Fast T	1.44	0.00	1.74	4.57	0.80	0.00	14.61
	θ_2	44.66	43.78	52.07	44.12	50.83	47.30	46.57
(90, 0)	L	1.00	0.00	0.00	10.00	0.00	1.00	5.00
	Slow T	1.83	2.00	1.99	0.00	11.90	3.00	0.00
	Fast T	2.00	0.00	0.00	0.00	0.00	1.00	0.00
(90, 45)	L	2.00	13.49	35.99	0.00	6.00	2.00	0.00
	Slow T	9.07	0.00	0.00	2.00	0.00	0.00	1.99
	Fast T	5.49	0.00	0.00	0.00	1.00	1.00	0.00
$(\theta_6, 45)$	L	···	1.50	1.75	···	3.75	1.50	···
	Slow T	···	0.00	0.00	···	0.00	0.00	···
	Fast T	···	1.18	2.06	···	1.08	2.26	···
	θ_6	···	24.04	39.83	···	62.02	50.26	···
$(\theta_2, 45)$	L	1.33	0.84	1.92	0.27	1.32	1.53	0.58
	Slow T	0.00	0.00	0.00	2.36	0.00	0.00	1.08
	Fast T	0.00	5.82	2.70	1.81	3.93	8.21	0.39
	θ_2	43.39	39.11	43.56	47.58	46.54	45.49	50.17

[a] TeO_2, paratellurite.
[b] KDP, potassium dihydrogen phosphate.

TABLE XIII. Approximate phonon-amplification factor in some cubic crystals. The entries are as described in Table XI.

(θ_v, ϕ_v)		CaF_2	Pb (at 0 °K)	LiF	MgO (at 4.2 °K)	Nb (at 4.2 °K)	Si	NaF
(0, 0)	L	4.00	0.00	0.00	1.00	4.00	1.00	4.00
	Slow T	0.00	0.00	15.00	42.55	0.00	6.00	0.00
	Fast T	0.00	1.00	9.00	19.00	0.00	11.00	0.00
(45, 0)	L	0.50	2.43	1.96	1.96	0.50	1.96	0.50
	Slow T	0.00	0.00	0.50	0.50	0.00	0.50	0.00
	Fast T	3.88	1.59	10.67	16.09	3.27	14.69	4.64
$(\theta_6, 45)$	L	0.25	2.49	2.24	2.24	0.50	2.24	0.25
	Slow T	3.16	0.00	1.76	3.23	2.40	1.76	4.93
	Fast T	0.00	0.00	0.00	0.00	0.98	0.00	0.00
	θ_6	54.74	54.74	54.74	54.74	54.74	54.74	54.74
$(\theta_2, 45)$	L	0.52	2.41	1.97	2.02	0.52	2.44	0.52
	Slow T	5.43	0.50	1.56	1.50	2.45	1.26	6.66
	Fast T	0.30	0.00	0.00	0.00	0.23	0.00	1.95
	θ_2	46.52	43.10	43.09	43.28	46.07	43.32	46.59

TABLE XIV. More accurate phonon-amplification factors, $A(\theta_v, \phi_v)$, along selected collinear axes for orthorhombic, tetragonal, and cubic materials whose elastic constants were determined at or below 4.2 °K. When the group-velocity spaces generated by the circular wave-vector spaces were quasielliptical, the PAF values given were calculated from their dimensions. The values marked with a dagger indicate that three wave-vector spaces gave rise to group-velocity vectors near the collinear axis. The value 0.1322 under calcium fluoride was not found by this method; it was obtained by numerical integration and agreed to within 1.3% of the value obtained when using Table V.

(θ_v, ϕ_v)		Ga	U	In	CaF_2	MgO	Si
(0, 0)	L	2.92	···	0.506	3.22	0.279	0.272
	Slow T	0.531	···	···	···	···	···
	Fast T	0.731	···	···	0.1322	···	···
$(\theta_6, 0)$	L	···	···	0.96	0.782	1.39	1.42
$(\theta_2, 0)$	Slow T	···	0.359	0.0613	···	···	···
	Fast T	0.605	···	···	3.10†	···	···
(90, 0)	L	0.559	···	0.42	···	···	···
	Slow T	0.772	···	···	···	···	···
	Fast T	5.27†	···	···	···	···	···
$(90, \phi_6)$	L	2.09	···	2.09	···	···	···
$(90, \phi_2)$	Slow T	0.262	0.272	0.190	···	···	···
	Fast T	···	···	···	···	···	···
(90, 90)	L	0.452	···	···	···	···	···
	Slow T	0.430	···	···	···	···	···
	Fast T	2.86†	···	···	···	···	···
$(\theta_2, 90)$	Slow T	···	0.203	···	···	···	···
	Fast T	0.826	···	···	···	···	···
$(\theta_6, 90)$	L	···	5.8	···	···	···	···
$(\theta_6, 45)$	L	···	···	···	0.445	2.12	2.16
$(\theta_2, 45)$	Slow T	···	···	0.051	···	0.441	0.311
	Fast T	···	···	···	···	···	···
(90, 45)	L	···	···	2.09	0.78	1.39	1.423
	Slow T	···	···	0.19	0.32	0.267	0.228
	Fast T	···	···	15.0	···	···	···

TABLE XV. Thermal conductivity, end-corrected mean free path, and thermal-conduction-enhancement factor for selected crystals at very low temperatures. Calculations were performed for samples in the form of circular cross-section rods with a thermal length of ten rod diameters. Symbols are defined in the text. The elastic constants used are those given in Table XVI.

Material	Lattice	Rod axis	κ/T^3 (W cm^{-1} °K^{-4})	Λ_{corr}/D	A_κ
Gallium	Orthorhombic	[001]	0.126	0.939	1.048
		[010]	0.134	0.996	1.045
		[100]	0.154	1.142	1.242
		[110]	0.106	0.789	0.809
Rutile	Tetragonal	[001]	0.0436	1.213	1.44
		[100]	0.0417	1.159	1.28
		[110]	0.0316	0.879	0.83
Magnesium oxide	Cubic	⟨100⟩	0.0340	1.31	1.45
		⟨110⟩	0.0247	0.95	0.98
		⟨111⟩	0.0231	0.893	0.95

TABLE XVI. Elastic constants of some orthorhombic, tetragonal, and cubic materials. All elastic constants are multiplied by 10^{11} for units of dyn/cm^2. The density is given in g/cm^3. All values are for measurements performed at room temperature, unless noted otherwise.

Orthorhombic material	C_{11}	C_{22}	C_{33}	C_{44}	C_{55}
Aragonite [a]	16.000	8.720	8.480	4.130	2.560
Barium sulphate [b]	8.620	9.170	10.840	1.200	2.870
Benzophenone [c]	1.070	1.000	0.710	0.203	0.155
Gallium (at 4.2 °K) [d]	11.180	9.960	14.780	3.970	4.520
Iodic acid [e]	3.012	5.805	4.286	1.688	2.065
Iodic acid (deuterated) [e]	3.009	5.800	4.281	1.692	2.064
Lithium ammonium [f] tartrate monohydrate	3.860	5.390	3.630	1.190	0.670
Magnesium sulphate [g] heptahydrate	3.250	2.880	3.150	0.780	1.560
Nickel sulphate [g] heptahydrate	3.530	3.110	3.350	0.910	1.720
Olivine [h]	32.400	19.800	24.900	6.670	8.100
Potassium pentaborate [i]	5.820	3.590	2.550	1.610	0.463
Resorcinol [j]	1.030	1.440	1.290	0.330	0.440
Rochelle salt [k]	4.060	5.200	6.400	1.220	0.300
Sodium ammonium [l] tartrate	3.680	5.090	5.540	1.060	0.303
Sodium tartrate [k]	4.610	5.470	6.650	1.240	0.310
Staurolite [m]	34.300	18.500	14.700	4.600	7.000
Strontium sulphate [b]	10.440	10.610	12.860	1.350	2.790
Sulfur [n]	1.422	1.268	1.830	0.827	0.428
Terpine monohydrate [o]	1.250	0.990	1.530	0.243	0.223
Topaz [p]	28.100	34.900	29.400	10.800	13.200
Uranium (at 4.2 °K) [q]	11.430	21.110	28.600	13.960	8.200
Zinc sulphate heptahydrate [g]	3.320	2.930	3.200	0.780	1.530

Tetragonal material	C_{11}	C_{33}	C_{44}
Ammonium dihydrogen [r] phosphate	6.890	3.350	0.856
Indium (at 4.2 °K) [s]	5.392	5.162	0.797
Indium bismuth [t]	5.110	3.460	1.980
Nickel sulphate [l] hexahydrate	3.210	2.930	1.160
Paratellurite [u]	5.570	10.580	2.650
Potassium dihydrogen [v] phosphate	7.400	6.800	1.350
Rutile [w]	26.600	46.990	12.390
White tin [x] (at 4.2 °K)	8.274	10.310	2.695
Zircon [y]	7.350	4.600	1.380

TABLE XVI. *(Continued)*

Orthorhombic material	C_{66}	C_{12}	C_{13}	C_{23}	ρ
Aragonite [a]	4.270	3.720	0.170	1.570	2.9300
Barium sulphate [b]	2.740	5.230	3.410	3.560	4.4320
Benzophenone [c]	0.353	0.550	0.169	0.321	1.2190
Gallium (at 4.2 °K) [d]	4.720	4.440	2.830	2.330	5.9840
Iodic acid [e]	1.582	1.608	1.106	0.796	4.6410
Iodic acid (deuterated) [e]	1.594	1.598	1.098	0.801	4.6670
Lithium ammonium [f] tartrate monohydrate	2.330	1.650	0.870	2.010	1.7100
Magnesium sulphate [g] heptahydrate	0.900	1.740	1.820	1.820	1.6770
Nickel sulphate [g] heptahydrate	0.990	1.980	2.010	2.010	1.9530
Olivine [h]	7.930	5.900	7.900	7.800	3.3240
Potassium pentaborate [i]	0.570	2.290	1.740	2.310	1.7400
Resorcinol [j]	0.400	0.620	0.740	0.690	1.2800
Rochelle salt [k]	0.950	2.560	3.460	3.200	1.7910
Sodium ammonium [l] tartrate	0.870	2.720	3.080	3.470	1.5900
Sodium tartrate [k]	0.980	2.860	3.200	3.520	1.7940
Staurolite [m]	9.200	6.700	6.100	12.800	3.3730
Strontium sulphate [b]	2.660	7.730	6.050	6.190	3.9600
Sulfur [n]	0.437	0.299	0.314	0.795	2.0750
Terpine monohydrate [o]	0.346	0.380	0.620	0.410	1.1100
Topaz [p]	13.100	12.600	8.400	8.800	3.5300
Uranium (at 4.2 °K) [q]	8.920	2.860	3.470	11.290	19.0400
Zinc sulphate heptahydrate [g]	0.830	1.720	2.000	1.980	1.9740

Tetragonal material	C_{66}	C_{12}	C_{13}	ρ
Ammonium dihydrogen [r] phosphate	0.595	0.400	1.890	1.7960
Indium (at 4.2 °K) [s]	1.684	3.871	4.513	7.4713
Indium bismuth [t]	1.590	3.700	3.200	8.9790
Nickel sulphate [l] hexahydrate	1.780	2.310	0.210	2.0700
Paratellurite [u]	6.590	5.120	2.180	5.9900
Potassium dihydrogen [v] phosphate	0.630	1.800	2.700	2.3380
Rutile [w]	18.860	17.330	13.620	4.2500
White tin [x] (at 4.2 °K)	2.818	5.785	3.421	7.3915
Zircon [y]	1.600	0.900	1.360	4.5931

TABLE XVI. (*Continued*)

Tetragonal material	C_{11}	C_{33}	C_{44}
Zirconium silicate [z]	42.370	49.000	11.360

Cubic material	C_{11}	C_{44}	C_{12}	ρ
Calcium fluoride [aa] (at 3 °K)	17.400	3.590	5.600	3.2100
Diamond [bb]	107.600	57.600	12.500	3.5120
Lead (at 0 °K) [cc]	5.554	1.942	4.542	11.5990
Lithium fluoride [dd]	12.460	6.490	4.240	2.6460

[a] W. Voigt, Ann. Phys. (Leipz.) 24, 290 (1907).
[b] T. Seshagiri Rao, Proc. Indian Acad. Sci. A 33, 251 (1951).
[c] A. A. Chumakov, I. M. Silvestrova, and K. S. Aleksandrov, Kristallografiya 2, 707 (1957) [Sov. Phys.-Crystallogr. 2, 699 (1957)].
[d] K. R. Lyall and J. F. Cochran, Can. J. Phys. 49, 1075 (1971).
[e] S. Haussuhl, Acta Crystallogr. A 24, 697 (1968).
[f] K. S. Aleksandrov and T. V. Ryzhova, Kristallografiya 6, 289 (1961) [Sov. Phys.-Crystallogr. 6, 228 (1961)].
[g] K. S. Aleksandrov, T. V. Ryzhova, and A. I. Rostuntseva, Kristallografiya 7, 930 (1962) [Sov. Phys.-Crystallogr. 7, 753 (1963)].
[h] R. K. Verma, J. Geophys. Res. 65, 757 (1960).
[i] W. R. Cook, Jr. and H. Jaffe, Acta Crystallogr. 10, 705 (1957).
[j] V. A. Koptsik, Kristallografiya 4, 219 (1959) [Sov. Phys.-Crystallogr. 4, 197 (1960)].
[k] R. V. G. Sundara Rao, Proc. Indian Acad. Sci. A 30, 173 (1949).
[l] R. F. S. Hearmon, Adv. Phys. 5, 323 (1956).
[m] J. Bhimasenachar and G. Venkata Rao, J. Acoust. Soc. Am. 29, 343 (1957).
[n] S. Haussuhl, Z. Naturforsch. A 24, 865 (1969).
[o] M. Silvestra, K. S. Aleksandrov, and A. A. Chumakov, Kristallografiya 3, 386 (1958) [Sov. Phys.-Crystallogr. 3, 388 (1958)].
[p] R. F. S. Hearmon, Rev. Mod. Phys. 18, 409 (1946).

small fraction of the superconducting transition temperature.

III. DISCUSSION

In the hexagonal lattice, because of transverse isotropy, all wave vectors occur in symmetry planes. As a result, general statements[13] concerning cuspidal edges (Sec. II D) and phonon focusing (Sec. II E and Appendix) are valid for all wave-vector directions in the lattice. In orthorhombic, tetragonal, and cubic lattices, however, such general statements are valid only when the wave vectors are confined to the symmetry planes of the lattice. Note also that since $a_7 > 0$, a collinear axis θ_s always exists for the slow mode in each of the symmetry planes. A number of solids do not have a collinear axis θ_f for the fast mode (see Tables VI–VIII) because focusing (defocusing) in the symmetry plane of the wave vectors does not occur both parallel and perpendicular to the η axis. It is also evident, that for wave vectors confined to a given symmetry plane, focusing (defocusing) of the T_1 mode in this plane about the η axis must result in defocusing (focusing) of this mode, for this plane, about $\eta_\perp$.

In orthorhombic lattices cusps about θ_2 in the (001) plane are very rare, occuring in only one material in Table VI, i.e., in potassium pentaborate. Cusps about θ_2 are more common in the other two symmetry planes. In the (100) plane they occur in 3 of the 22 materials listed, and in the (010) plane they occur in 9 of the 22. Eight of the orthorhombic materials, however, have cusps about both the [100] and [010] directions in the (001) plane.

In tetragonal materials, however, cusps about θ_2 in the (001) plane are far more frequent than they are in orthorhombic materials. They occur in nearly half the tetragonal materials in Table VII. Further consideration reveals that cusps about θ_2 are almost evenly distributed among the (010), (110), and (001) planes. Cusps about the [001] axis are rather rare and exist in only two of the tetragonal materials of Table VII because only indium and indium bismuth, show a θ_0 value in the (010) or the (110) planes. Indium, indium bismuth, and rutile are the only tetragonal materials listed which have a cusp about the [100] direction in the

TABLE XVI. (*Continued*)

Tetragonal material	C_{66}	C_{12}	C_{13}	ρ
Zirconium silicate [z]	4.850	7.030	14.950	4.5310
Cubic material	C_{11}	C_{44}	C_{12}	ρ
Magnesium oxide [ee] (at 4.2 °K)	30.670	15.760	9.371	3.5800
Niobium (at 4.2 °K) [ff]	25.231	2.998	13.617	8.6206
Silicon (at 3 °K) [gg]	16.770	8.040	6.500	2.3301
Sodium fluoride [hh]	10.850	2.900	2.290	2.8510

[q] E. S. Fisher and D. Dever, Phys. Rev. 170, 607 (1968).
[r] W. J. Price and H. B. Huntington, J. Acoust. Soc. Am. 22, 32 (1950).
[s] B. S. Chandrasekhar and J. A. Rayne, Phys. Rev. 124, 1011 (1961).
[t] Y. C. Akgoz, J. M. Farley, and G. A. Saunders, J. Phys. Chem. Solids 34, 141 (1973).
[u] Y. Ohmachi and N. Uchida, J. Appl. Phys. 41, 2307 (1970).
[v] H. M. Barkla and D. M. Finlayson, Philos. Mag. 44, 109 (1953).
[w] J. B. Wachtman, Jr., W. E. Tefft, and D. G. Lam, Jr., J. Res. Natl. Bur. Stand. (U.S.) A 66, 465 (1962).
[x] J. A. Rayne and B. S. Chandrasekhar, Phys. Rev. 120, 1661 (1960).
[y] J. Bhimasenachar and G. Venkataratnam, J. Acoust. Soc. Am. 27, 922 (1955). Value of C_{13} was corrected by Ref. f.
[z] H. Ozcan, L. Cartz, and J. Jamieson, J. Appl. Phys. 45, 556 (1974).
[aa] D. R. Huffmann and M. H. Norwood, Phys. Rev. 117, 709 (1960).
[bb] H. J. McSkimin and W. L. Bond, Phys. Rev. 105, 116 (1957).
[cc] D. L. Waldorf and G. A. Alers, J. Appl. Phys. 33, 3268 (1962).
[dd] C. V. Briscoe and C. F. Squire, Phys. Rev. 106, 1175 (1957).
[ee] K. Marklund and S. A. Mahmoud, Phys. Scr. 3, 75 (1971).
[ff] Calculated using phonon velocities from R. Weber, Phys. Rev. 133, A1487 (1964).
[gg] H. J. McSkimin and P. Andreatch, J. Appl. Phys. 35, 2161 (1964).
[hh] J. T. Lewis, A. Lehoczsky, and C. V. Briscoe, Phys. Rev. 161, 877 (1967).

(010) plane. Notice that of the tetragonal materials listed only indium bismuth has a cusp about the [110] direction in the (110) plane. Cusps about the [100] and [010] axes in the (001) plane, however, are quite common, occurring in six of the ten materials listed.

Cusps in the group-velocity surface of the T_1 mode are always absent for wave vectors in symmetry planes (see Theorem III). Cuspidal edges in the T_1 group-velocity surface, however, can exist for wave vectors in orthogonally intersecting, nonsymmetry planes. As a result, considerable care must be exercised before a group-velocity surface is given a cusp-free designation. Consider, for example, the phase-velocity surface of orthorhombic gallium in Fig. 1. Note that the T_2 portion of the ρs^2 surface in the (001) plane meets the T_1 portion in the (010) plane at the [100] axis, and the T_1 portion in the (100) plane at the [010] axis. Because a cusp exists about the [100] axis in the (001) plane (see Table VI), symmetry considerations require that group velocities in the (010) plane can also be generated by wave vectors on either side of the (010) plane. These group velocities form a second (inner) locus in the (010) plane and form part of the cuspidal configuration which extends from the [100] axis toward the [001] direction on both sides of the (010) plane. A similar situation occurs about the [010] axis where, because of the cuspidal edge in the (001) plane about the [010] axis, the cuspidal configuration extends from the [010] axis toward the [001] direction on both sides of the (100) plane. In tetragonal indium, there is, in addition, a cuspidal edge about the [100] axis in the (010) plane, and about the [010] axis in the (100) plane (see Table VI), so that a cuspidal configuration extends from the [100] axis to the [010] axis on both sides of the (001) plane. Similarly, in cubic calcium fluroride, the cuspidal edge shown in Fig. 7 around the [100] axis is part of the cuspidal configuration about the [011] axis in the (100) plane which extends from the [011] axis toward the [100] direction.

Note that the presence of cuspidal edges can give rise to a large phonon-amplification factor. The amount of enhancement is related to the width

of the cusp (the narrower the cusp the higher the phonon intensity). The highest phonon intensities in Tables IX and X occur where the direction of the group velocity varies on the average most slowly with wave-vector direction within the 2° mesh used in the computer calculations. For some of the materials listed in Tables IX and X this occurs in the vicinity of a cusp (see Tables VI–VIII), but for others where conditions for a cusp are nearly satisfied.

A cusp in a symmetry plane about a principal axis may not give a high phonon intensity within a 1° deviation from that axis if the group-velocity direction varies quite rapidly with wave-vector direction in the other symmetry plane. Gallium, for example, has a cusp about the [010] axis in the (001) plane (see Table VI), but in the (100) plane near the [010] direction calculations show that the group-velocity direction varies more than twice as rapidly as the wave-vector direction. It should not be surprising, therefore, that the resulting phonon intensity along the [010] axis is only unity.

However, high phonon intensities can exist in the absence of a cusp if the group-velocity direction varies slowly with wave-vector direction in both symmetry planes. Orthorhombic aragonite gives a good example of this (see Tables VI and XI.) There is no cusp about its [010] axis, but near this axis the group-velocity directions for both transverse modes varies slowly with wave-vector direction in both the (001) and (100) planes. The result is a phonon intensity along the [010] axis of 23.8 for the slow transverse mode and 4.0 for the fast transverse mode. High intensities can also occur in the longitudinal mode when the group-velocity direction varies slowly with wave vector. An excellent example is paratellurite in the (001) plane, where conditions for a cuspidal edge about $\theta_f = 45°$ in the fast mode are more favorable than in any other known material.

Note that the orthorhombic lattice can not have double cusps along its principal axes generated by wave vectors confined to symmetry planes. This is evident from Fig. 1 which shows that for a given surface, a T_2 portion in one symmetry plane always meets a T_1 portion in the adjoining symmetry plane. However, double cusps can exist along the [001] axis in tetragonal and cubic crystals even when wave vectors are confined to symmetry planes. In fact, indium has a cusp along the [001] direction in all symmetry planes which contain the [001] direction. This is possible because, as is shown in Fig. 2, all T_2 portions on symmetry planes can meet at a common point along the [001] axis in tetragonal and cubic crystals. Figure 2 also indicates that double cusps can not exist along the [100], [110], and [010] directions in a tetragonal crystal (when wave vectors are confined to symmetry planes) because, for a given surface along these directions, all T_2 portions in symmetry planes meet T_1 portions.

Materials for which the ratios of the elastic constants are similar have similar anisotropies and focusing properties. Cubic materials, for example, with similar anisotropies have many similar PAF values (see Table XIII). Table VIII shows that calcium fluoride, niobium, and sodium fluoride (which shall be designated Set A) all have cusps about the ⟨110⟩ directions and near the ⟨111⟩ directions, while lead, lithium fluoride, magnesium oxide, and silicon (designated as Set B) all have cusps about the ⟨100⟩ and ⟨110⟩ directions. As a result energy flow is enhanced along the ⟨100⟩ and ⟨110⟩ directions in Set B, but along the ⟨111⟩ and ⟨110⟩ directions in Set A. Thus for Set B the thermal conductivity is larger along the ⟨100⟩ and ⟨110⟩ directions than along the ⟨111⟩ directions and for Set A higher along the ⟨111⟩ and ⟨110⟩ directions than along the ⟨110⟩ directions.[12,14]

Furthermore, calculations of A_κ show that the effects of focusing can actually reverse the anisotropy one obtains by neglecting the angular deviation between the phase and group velocities. For example, magnesium oxide would have a thermal conductivity κ_s of 0.0234 in the ⟨100⟩ directions and 0.0244 in the ⟨111⟩ directions if focusing were neglected, but when focusing effects are considered the correct thermal conductivity κ_v is 0.0340 in the ⟨100⟩ directions and 0.0231 in the ⟨111⟩ directions. Similarly, for rutile, κ_s is 0.0303 and 0.0381 for the [001] and [110] directions, respectively, but the correct thermal conductivity κ_v is 0.0436 and 0.0316, respectively, for these same directions.

Finally, note that phonon focusing, a general property of elastically anisotropic crystals, also occurs in crystal lattices of still lower symmetry. Strong focusing is predicted to have a dramatic effect upon the phonon conductivity at very low temperatures provided the phonon mean free path can approach sample dimensions.

ACKNOWLEDGMENTS

The authors wish to express their appreciation to the Worcester Area College Computation Center at Worcester Polytechnic Institute, and to the University of Evansville Computer Center for the use of their computing facilities.

IV. APPENDIX

Since group-velocity vectors in a symmetry plane can be generated by wave vectors on either

side of that symmetry plane, the following three theorems assume that the wave vectors, and thus their corresponding group-velocity vectors are restricted to the symmetry planes of the crystal lattice.

Theorem I. If a collinear axis θ_f in a symmetry plane exists, any focusing (defocusing) occurring about θ_f in the fast mode must be accompanied by defocusing (focusing) of the fast mode about both η and $\eta_\perp$ axes, and conversely.

For focusing (defocusing) of the fast mode about θ_f,

$$|a_7|[(|a_7|-a_5)+(|a_7|-a_6)] \times[\tfrac{1}{2}(a_4+a_6)(a_6-a_5)+(|a_7|+a_4)(|a_7|-a_6)]>0.$$

Proof: From Figs. 3 and 4, based upon Eqs. (20)–(22), it is self-evident that for a θ_f to exist, and for focusing (defocusing) to occur about θ_f, that the values of θ_v versus θ_k must intersect the line $\theta_v = \theta_k$ at $\theta_k = \theta_f$. Since η and $\eta_\perp$ are the only other collinear axes for the fast mode, focusing (defocusing) about θ_f must thus be accompanied by defocusing (focusing) about both η and $\eta_\perp$, and conversely.

For a θ_f to exist, Eq. (26) requires

$$(|a_7|-a_6)(|a_7|-a_5)>0. \tag{A1}$$

Furthermore, for a θ_f to exist, and for defocusing to occur about η and $\eta_\perp$, inequality (A1) and Sec. II E require

$$(|a_7|-a_6)(|a_7|-a_5)(a_7^2-a_5a_6)>0, \tag{A2}$$

but for focusing about these same two directions requires

$$(|a_7|-a_6)(|a_7|-a_5)(a_7^2-a_5a_6)<0. \tag{A3}$$

Because of Eq. (48) and inequalities (A2) and (A3), respectively, both focusing (defocusing) about θ_f require

$$|a_7|[(|a_7|-a_5)+(|a_7|-a_6)] \times[\tfrac{1}{2}(a_4+a_6)(a_6-a_5)+(|a_7|+a_4)(|a_7|-a_6)]>0. \tag{A4}$$

Theorem II. If a collinear axis θ_s in a symmetry plane exists, any focusing or cuspidal edge occurring in the slow mode about θ_s must be accompanied by defocusing of the slow mode about both η and $\eta_\perp$. Similarly, any defocusing of the slow mode about θ_s must be accompanied by focusing at both η and $\eta_\perp$, or a cuspidal edge about either η or $\eta_\perp$ or both axes. The converse of the two previous statement is also true.

For a cuspidal edge, or focusing (defocusing) of the slow mode about θ_s

$$|a_7|[(a_5+|a_7|)+(a_6+|a_7|)] \times[\tfrac{1}{2}(a_4+a_6)(a_5-a_6)+(a_4-|a_7|)(a_6+|a_7|)]>0.$$

Proof: From Figs. 3 and 4, based upon Eqs. (20)–(22), it is self-evident that for a θ_s to exist, and for a cuspidal edge or focusing (defocusing) to occur about θ_s, that the values of θ_v versus θ_k must intersect the line $\theta_v = \theta_k$ at $\theta_k = \theta_s$. Since η and $\eta_\perp$ are the only other collinear axes for the slow mode, a cuspidal edge or focusing about θ_s must be accompanied by defocusing about both η and $\eta_\perp$, and conversely. Similarly, defocusing of the slow mode about θ_s must be accompanied by focusing of the slow mode about both η and $\eta_\perp$, or a cuspidal edge about either η or $\eta_\perp$ or both axes, depending upon the strength of the inequality $a_7^2 > a_5a_6$. Conversely, focusing of the slow mode about both η and $\eta_\perp$, or a cuspidal edge about either η or $\eta_\perp$ or both axes, must be accompanied by defocusing of the slow mode about θ_s.

For a θ_s to exist, Eq. (25) requires

$$(a_5+|a_7|)(a_6+|a_7|)>0. \tag{A5}$$

Also, for a cuspidal edge about θ_s or for focusing about θ_s, defocusing must occur about both η and $\eta_\perp$. Together with inequality (A5) this requires

$$(a_5+|a_7|)(a_6+|a_7|)(a_5a_6-a_7^2)>0, \tag{A6}$$

but for focusing about these same two directions requires

$$(a_5+|a_7|)(a_6+|a_7|)(a_5a_6-a_7^2)<0. \tag{A7}$$

Because of Eq. (47) and inequalities (A6) and (A7), respectively, both focusing (and defocusing) about θ_s require

$$|a_7|[(a_5+|a_7|)+(a_6+|a_7|)] \times[\tfrac{1}{2}(a_4+a_6)(a_5-a_6)+(a_4-|a_7|)(a_6+|a_7|)]>0. \tag{A8}$$

Theorem III. Cuspidal edges in the transverse T_1 mode, and the fast mode about any collinear point in a symmetry plane, are always absent in an elastically stable solid.

Proof: For the T_1 mode in any symmetry plane

$$\frac{d\theta_k}{d\theta_v}=\frac{a_2\sec^2\theta_v}{a_1\sec^2\theta_k}. \tag{A9}$$

Since $a_1>0$, $a_2>0$ therefore, $d\theta_k/d\theta_v>0$ for all values of θ_k, and a cuspidal edge is impossible. For the fast mode a cuspidal edge about the η axis requires

$$\frac{a_4+|a_6|}{a_3+(2a_7^2-a_5a_6)/|a_6|}<0.$$

Since $a_4+|a_6|>0$, this requires

$$a_3 + (2a_7^2 - a_5 a_6)/|a_6| < 0$$

or

$$2a_7^2 < a_5 a_6 - a_3 |a_6| \tag{A10}$$

If $a_6 > 0$, then a cuspidal edge requires $2a_7^2 < a_6(a_5 - a_3)$ which is impossible since $a_6 > 0$ and $(a_5 - a_3) < 0$ for all symmetry planes. If $a_6 < 0$, then a cuspidal edge requires $2a_7^2 < a_6(a_5 + a_3)$ which again is impossible since $(a_5 + a_3) > 0$ and $a_6 < 0$.

For a cuspidal edge about the $\eta_\perp$ axis the proof is similar but with a_3 replacing a_4, and with a_5 and a_6 interchanged. Results for a_5, $a_6 > 0$ and for the T_1 mode were previously proved by Musgrave,[11] by considering the inverse phase-velocity surface.

For a cuspidal edge to exist about θ_f, Eq. (48) and inequalities (A2) and (A4) require

$$4(|a_7| - a_6)(|a_7| - a_5)(a_7^2 - a_5 a_6) > |a_7|[(|a_7| - a_5) + (|a_7| - a_6)] \times [\tfrac{1}{2}(a_4 + a_6)(a_6 - a_5) + (|a_7| + a_4)(|a_7| - a_6)] . \tag{A11}$$

Since a cuspidal edge about θ_f requires defocusing about both η and $\eta_\perp$, inequality (A1) and Sec. II E require

$$(|a_7| - a_5) + (|a_7| - a_6) > 0 \tag{A12}$$

and because of inequality (A4) requires

$$\tfrac{1}{2}(a_4 + a_6)(a_6 - a_5) + (|a_7| + a_4)(|a_7| - a_6) > 0 . \tag{A13}$$

Inequality (A13) reduces to the following conditions for each of the symmetry planes of the orthorhombic lattice. For the (010) plane:

$$(C_{13} + 2C_{55})^2 - C_{11}C_{33} > 0 \quad \text{if} \quad a_7 > 0 , \tag{A14}$$

but

$$C_{13}^2 - C_{11}C_{33} > 0 \quad \text{if} \quad a_7 < 0 ; \tag{A15}$$

the (100) plane:

$$(C_{23} + 2C_{44})^2 - C_{22}C_{33} > 0 \quad \text{if} \quad a_7 > 0 , \tag{A16}$$

but

$$C_{23}^2 - C_{22}C_{33} > 0 \quad \text{if} \quad a_7 < 0 ; \tag{A17}$$

the (001) plane:

$$(C_{12} + 2C_{66})^2 - C_{11}C_{22} > 0 \quad \text{if} \quad a_7 > 0 , \tag{A18}$$

but

$$C_{12}^2 - C_{11}C_{22} > 0 \quad \text{if} \quad a_7 < 0 ; \tag{A19}$$

and for the (110) plane of the tetragonal lattice to

$$(C_{13} + 2C_{44})^2 - C_{33}[\tfrac{1}{2}(C_{11} + C_{12}) + C_{66}] > 0 \quad \text{if} \quad a_7 > 0 , \tag{A20}$$

but

$$C_{13}^2 - C_{33}[\tfrac{1}{2}(C_{11} + C_{12}) + C_{66}] > 0 \quad \text{if} \quad a_7 < 0 . \tag{A21}$$

Inequalities (A15), (A17) and (A19) violate conditions (6), and (A21) violates condition (11) for elastic stability. Inequalities (A14), (A16), (A18) and (6) give the necessary but not sufficient conditions on a_7 for a cusp about θ_f in the orthorhombic lattice. For the (010) plane:

$$C_{13} + C_{55} > (C_{11}C_{33} - C_{13}^2)/4C_{55} > 0 , \tag{A22}$$

the (100) plane:

$$C_{23} + C_{44} > (C_{22}C_{33} - C_{23}^2)/4C_{44} > 0 , \tag{A23}$$

and the (001) plane:

$$C_{12} + C_{66} > (C_{11}C_{22} - C_{12}^2)/4C_{66} > 0 . \tag{A24}$$

Similarly, inequalities (A20) and (11) give the necessary but not sufficient conditions on a_7 for a cusp about θ_f in the (110) plane of the tetragonal lattice:

$$C_{13} + C_{44} > \{C_{33}[\tfrac{1}{2}(C_{11} + C_{12}) + C_{66}] - C_{13}^2\}/4C_{44} > 0 . \tag{A25}$$

Necessary but not sufficient conditions on a_7 for a cusp about θ_f for the other symmetry planes of tetragonal, hexagonal and cubic lattices are easily obtained from inequalities (A22)–(A25).

Since $a_7 > 0$, a cusp, if one exists about θ_f, will most likely occur when $a_7 \gg |a_5|$, $a_7 \gg |a_6|$. For finite a_7, the most extreme case consistent with elastic stability occurs when $a_5 = a_6 = 0$, for which inequality (A11) reduces to $2a_7 > a_7 + a_4$. Inequality (A26) is impossible to satisfy since $a_4 > a_7$ when $a_5 = a_6 = 0$ for all symmetry planes in an elastically stable solid.

---

*Based on a thesis submitted by C. G. Winternheimer, in partial fulfillment of the requirements for the Ph.D. degree at Worcester Polytechnic Institute.

†Permanent address: Dept. of Electrical Engineering, University of Evansville, Evansville, Ind. 47712.

[1]For a general review, see J. M. Ziman, *Electrons and Phonons* (Oxford U.P., London, 1960); P. Carruthers, Rev. Mod. Phys. 33, 92 (1961); P. G. Klemens, in *Solid State Physics*, edited by F. Seitz and D. Turnbull (Academic, New York, 1958), Vol. 7, p. 1; Paper No. 66-9F5-TPROP-P5 Westinghouse Research Laboratories Library, Pittsburg, Penn., 1966 (unpublished).

[2]H. B. G. Casimir, Physica (Utr.) 5, 495 (1938).

[3]R. Berman, F. E. Simon, and J. M. Ziman, Proc. R. Soc. A 220, 171 (1953).

[4]R. Berman, E. L. Foster, and J. M. Ziman, Proc. R. Soc. A 231, 130 (1955).
[5]A. K. McCurdy, H. J. Maris, and C. Elbaum, Phys. Rev. B 2, 4077 (1970).
[6]A. K. McCurdy, Ph.D. thesis (Brown University, 1971) (unpublished) (University Microfilms, Inc., Ann Arbor, Michigan, Order No. 72-12,047).
[7]J. Bardeen, L. N. Cooper, and J. R. Schrieffer, Phys. Rev. 106, 162 (1957); *ibid.* 108, 1175 (1957).
[8]A. C. Anderson, C. B. Satterthwaite, and S. C. Smith, Phys. Rev. B 3, 3762 (1971).
[9]B. Taylor, H. J. Maris, and C. Elbaum, Phys. Rev. Lett. 23, 416 (1969).
[10]B. Taylor, H. J. Maris, and C. Elbaum, Phys. Rev. B 3, 1462 (1971).
[11]M. J. P. Musgrave, Proc. Camb. Philos. Soc. 53, 897 (1957).
[12]H. J. Maris, J. Acoust. Soc. Am. 50, 812 (1971).
[13]A. K. McCurdy, Phys. Rev. B 9, 466 (1974).
[14]C. G. Winternheimer and A. K. McCurdy, Solid State Commun. 14, 919 (1974).
[15]V. Narayanamurti and R. C. Dynes, Phys. Rev. B 12, 1731 (1975).
[16]See, for example, L. D. Landau and E. M. Lifshitz, *Theory of Elasticity* (Addison-Wesley, Reading, Mass., 1959), p. 105.
[17]M. J. P. Musgrave, Proc. R. Soc. A 226, 356 (1954).
[18]F. I. Fedorov, *Theory of Elastic Waves in Crystals* (Plenum, New York, 1958), pp. 215–219.
[19]C. G. Winternheimer, Ph.D. thesis (Worcester Polytechnic Institute, 1975) (unpublished).
[20]See, for example, Ref. 18, pp. 215–219.
[21]Note that in Table I $a_3-a_4=a_5-a_6$.
[22]For most materials the subscripts 0, 1 and 2 can be designated as L, T_1 and T_2, respectively.
[23]Reference 18, p. 16.
[24]Although a_7 may be positive or negative in principle, the mode designations used in Secs. III B and III C are shown in the Appendix to require $a_7>0$.
[25]G. Arlt and H. Schweppe, Solid State Commun. 6, 783 (1968).
[26]Y. Ohmachi, N. Uchida, and N. Niizeki, J. Acoust. Soc. Am. 51, 164 (1972).
[27]A mode will be considered quasitransverse if the angle between the polarization vector and the wave vector is greater than 45° but less than 135°.
[28]Reference 18, p. 124.
[29]R. C. Addison, B. A. Auld, and J. H. Wilkinson, Proc. IEEE 55, 68 (1967).
[30]Y. Kikucki, N. Chubacki, and H. Sasaki, IEEE Trans. Sonics Ultrason. 16, 200 (1969).
[31]K. Brugger, J. Appl. Phys. 36, 759 (1965).
[32]Magnitude bars must be placed on a_7 to prevent an interchange of the two roots when considering the case $a_7<0$.
[33]F. E. Borgnis, Phys. Rev. 98, 1000 (1955).
[34]A discussion of cusp-free velocity surfaces is given in Sec. III.
[35]Note that along the [001] axis the tetragonal and cubic lattices have two sets of mutually orthogonal symmetry planes. This case is discussed in more detail in a later paragraph.
[36]This applies only to the [100], [010], and [001] axes. The case for other collinear axes, which have only one symmetry plane, are discussed in a later paragraph.
[37]In paper I and in Fig. 4, θ_s and θ_f are designated as θ_2 and θ_6, respectively.
[38]This is a direct result of the interchange of the roots for the collinear points for values of $a_7<0$. Magnitude bars on a_7 are unnecessary if a_7 is restricted to $a_7>0$.
[39]See, for example, *Handbook of Mathematical Functions with Formulas, Graphs, and Mathematical Tables*, edited by M. Abramowitz and I. Stegun, Natl. Bur. Stand. Appl. Math. Ser. 55 (U.S. GPO, Washington, D.C., 1964), p. 17.